Meiotic Cells Counteract Programmed Retrotransposon Activation via RNA-Binding Translational Repressor Assemblies

TITLE

Meiotic cells counteract programmed retrotransposon activation via RNA-binding translational repressor assemblies

AUTHOR LIST AND AFFILIATIONS

Raphaelle Laureau[1], Annie Dyatel[1], Gizem Dursuk[1], Samantha Brown[1], Hannah Adeoye[1], Jia-Xing Yue[2], Matteo De Chiara[2], Anthony Harris[3], Elçin Ünal[3], Gianni Liti[2], Ian R. Adams[4], Luke E. Berchowitz[1,5,*]

[1] Department of Genetics and Development, Hammer Health Sciences Center, Columbia University Irving Medical Center, New York, NY 10032, USA.
[2] Université Côte d'Azur, CNRS, Inserm, IRCAN, Nice 06107, France.
[3] Department of Molecular and Cell Biology, University of California, Berkeley, Berkeley, CA 94720, USA.
[4] MRC Human Genetics Unit, MRC Institute of Genetics and Molecular Medicine, University of Edinburgh EH4 2XU, Edinburgh, United Kingdom.
[5] Lead Contact

*Correspondance: leb2210@cumc.columbia.edu

Luke E. Berchowitz, Ph.D.
701 W 168th St. Hammer Health Sciences Building Room 1520
Columbia University Irving Medical Center
New York NY, 10032
Phone: 212-305-7003

SUMMARY

Retrotransposon proliferation poses a threat to germline integrity. While retrotransposons must be activated in developing germ cells in order to survive and propagate, how they are selectively activated in the context of meiosis is unclear. We demonstrate that transcriptional activation of *Ty3*/*Gypsy* retrotransposons and host defense are controlled by master meiotic regulators. We show that budding yeast *Ty3/Gypsy* co-opts binding sites of the essential meiotic transcription factor Ndt80 upstream of the integration site, thereby tightly linking its transcriptional activation to meiotic progression. We also elucidate how yeast cells thwart *Ty3/Gypsy* proliferation by blocking translation of the retrotransposon mRNA using amyloid-like assemblies of the RNA-binding protein Rim4. In mammals, several inactive *Ty3/Gypsy* elements are undergoing domestication. We show that mammals utilize equivalent master meiotic regulators (Stra8, Mybl1, Dazl) to regulate *Ty3/Gypsy*-derived genes in developing gametes. Our findings inform how genes that are evolving from retrotransposons can build upon existing regulatory networks during domestication.

INTRODUCTION

The relationship between organisms and transposable elements is complex and fluctuating. For the organism, transposable elements can act as a reservoir for novel genes and drive genomic plasticity, but they are also key drivers of genome instability. Insertions can rearrange regulatory networks and alter gene expression patterns (Chuong et al., 2017; Mita and Boeke, 2016; Rebollo et al., 2012). More dangerously, insertion of transposable elements can disrupt genetic information, give rise to heterologies, and can potentially provide sites for ectopic recombination (Warren et al., 2015). For the element, if it is to survive and proliferate, it must do so with minimal detriment and possible benefit to the host (Cosby et al., 2019; Haig, 2016).

Retrotransposons are a class of transposable elements that propagate through an RNA intermediate via a copy and paste mechanism. This mechanism preserves the original element while generating DNA copies which are free to invade other loci. Retrotransposon proliferation has seemingly no intrinsic limit and poses an acute burden to the host genome. This burden is reflected in the repetitive fraction of genomes, which is primarily composed of retrotransposon-derived sequences. In this study we focus on understanding the biology underpinning proliferation of a class of Long-Terminal-Repeats retrotransposons (LTR-retrotransposons), *Ty3/Gypsy*, during meiosis.

LTR-retrotransposons are divided into four superfamilies based on structure and phylogeny: *Ty1/Copia*, *Ty3/Gypsy* (both represented in all eukaryotic lineages), *Bel-Pao* (found in metazoans but not mammals), and ERVs (Endogenous RetroViruses, found only in vertebrates) (Wicker et al., 2007). *Ty3/Gypsy* and ERVs are closely related because many vertebrate retroviruses likely arose from *Ty3/Gypsy* retrotransposons that acquired the envelope gene from other viruses (Hayward, 2017). Although no active *Ty3/Gypsy* retrotransposons are found in mammalian genomes, several sequences derived from *Ty3/Gypsy* are present, many of which have been domesticated for cellular functions (Volff, 2009).

The *Ty3/Gypsy* life cycle is much like that of a retrovirus except it occurs entirely within the cell. It is transcribed into an mRNA which encodes 2 polyproteins: Gag3 and Gag3-Pol3 (**Figure 1A**). Gag3 is the precursor to the capsid (CA) and nucleocapsid (NC) proteins and Pol3 is the precursor to a protease (PR), a reverse transcriptase-RNaseH (RT-RH), and an integrase (IN). In most cases only Gag3 polyprotein is translated, while Gag3-Pol3 is only produced by a frameshift that occurs in 5-10% of translation events (Farabaugh et al., 1993) (**Figure 1A**). Gag3 assembles together with a *Ty3* mRNA dimer and Gag3-Pol3 into a remarkable structure within the cell – the virus-like particle (VLP) – inside which the precursor proproteins mature into their final products and the *Ty3* mRNA is reverse transcribed into cDNA (Garfinkel et al., 1985). This cDNA copy is bound to integrase proteins and can

enter the nucleus via the nuclear pore to integrate in the genome. *Ty3* integration events require binding to polymerase III and thus frequently occur in close proximity to tRNA genes (Qi et al., 2012).

For a retrotransposon to increase its copy number and proliferate through generations it must to do so in cells that will ultimately become gametes. For this reason, retrotransposons tend to be expressed in the developing germline, including during meiosis (Crichton et al., 2014; Ribeiro-dos-Santos et al., 1997). However, as retrotransposon mobilization in these cells can cause heritable mutations and trans-generational genetic instability, organisms have evolved elegant multi-layered mechanisms which act at various stages of the retrotransposon cycle to protect their germlines (Crichton et al., 2014).

For example, transcription of retrotransposons can be repressed by DNA methylation, chromatin modifications, and transcriptional interference (for review (Crichton et al., 2014; Yang and Wang, 2016)). Post-transcriptional pathways such as miRNA, siRNA, piRNA target retrotransposon mRNA for degradation (Bao and Yan, 2012; Dechaud et al., 2019; Yang and Wang, 2016) and RNA modification enzymes such as cytidine deaminases prevent reverse transcription of the retrotransposon mRNA into cDNA (Orecchini et al., 2018). Post-translational regulatory mechanisms act in germ cells to target retrotransposon proteins for premature degradation (MacLennan et al., 2017). Beyond the obvious long-term consequences of uncontrolled retrotransposon proliferation, dysregulation of retrotransposon control can cause acute failures in gamete development. Disruption of defense mechanisms in mice or *Drosophila* leads to sterility (Barau et al., 2016; Bourc'his and Bestor, 2004; Wang et al., 2018) and hyperactivation of retrotransposons causes fetal oocyte attrition in mice (Malki et al., 2014).

Here, we show that *Ty3/Gypsy* elements can exploit the genomic environment at their integration sites to ensure transcriptional activation during the meiotic divisions. Our results illustrate a mechanism by which retrotransposons can restrict their expression to a developmental context in which activation is beneficial. We also identify an opposing mechanism by which cells defend their genome against meiotic retrotransposition. Developing budding yeast *Saccharomyces cerevisiae* gametes utilize amyloid-like RNA-binding protein assemblies to repress *Ty3* translation thereby halting the proliferation cycle. We find that both the co-opting of meiotic regulators by *Ty3/Gypsy* elements and their interaction with assembly-forming RNA-binding proteins are strategies which are also employed by *Gypsy*-derived genes in mammals. Our findings highlight the likely hundreds of millions of years of perpetual interactions among retrotransposons, host RNA-binding proteins, and genomes.

RESULTS

Ty3 is expressed in coordination with meiotic progression

We first determined whether retrotransposons are transcriptionally active during *S. cerevisiae* meiosis (strains used in this study are described in **Table S1**). We performed RNAseq at hourly time points from cells undergoing synchronous meiosis using the *NDT80* block-release system (Benjamin et al., 2003; Carlile and Amon, 2008). There is only one full-length copy of *Ty3* in the SK1 strain, and we observed that this locus is transcribed in the sense orientation specifically during the meiotic divisions (**Figure 1A, B**). We also observed an antisense RNA at the onset of meiosis that declines as meiosis proceeds to almost undetectable levels. These data led us to hypothesize that transcription of the full-length *Ty3* is repressed in mitotic cells but is activated during the meiotic divisions.

Only a full-length retrotransposon mRNA can complete the steps necessary for proliferation. While our RNAseq data imply that the *Ty3* locus is transcribed in meiosis, we sought to differentiate whether this was indicative of bona-fide full-length transcripts or of cryptic inactive transcripts that span the locus. Using Northern blot analysis, we observed several *Ty3* RNA isoforms (**Figure 1C**), consistent in size with the various isoforms spanning the locus in the RNAseq (**Figure 1B**), including a prominent band of the size of a full-length transcript (5 kb). All of the RNA isoforms we observed were specific to *Ty3* because none of them were produced in cells lacking *Ty3* (*ty3*Δ) (**Figure 1C, Figure S1A, B**). Using probe tiling, we were able to identify this top band as a full-length mRNA, containing both *GAG3* and *POL3* coding sequences (**Figure S1C**) and thus the potential capacity to propagate. Strikingly, full-length *Ty3* mRNA was expressed and reached maximal levels at the first meiotic division (**Figure 1C, D**).

We next determined whether meiotic transcriptional activation of *Ty3* occurs in other *S. cerevisiae* isolates. Because rapid, efficient, and synchronous meiosis is a feature that is not shared by most lab strains, we decided to investigate a collection of wild diploid isolates (Peter et al., 2018) for sporulation efficiency and *Ty3* activation (**Table S2**). These strains harbor varying *Ty3* copy numbers. We found that full-length *Ty3* transcription switches on at the time of meiotic divisions in at least one isolate, OS673, which harbors two full-length copies of *Ty3* (**Figure 1E-G, Table S2**). This strain was isolated from a beetle in Hungary (Peter et al., 2018) and is of a completely different genetic background than SK1 (~ 51,400 SNPs), allowing us to rule out the possibility that *Ty3* activation in meiosis is a peculiarity that appeared during lab domestication. From these data we conclude that *Ty3* retrotransposons have evolved to activate, and potentially proliferate, during meiosis.

Ty3 expression is controlled by a critical meiotic transcription factor

How is *Ty3* transcription activated specifically at the onset of meiosis I? The transition from meiotic prophase to the first meiotic division is governed by the meiosis-specific transcription factor Ndt80 (Xu et al., 1995). Accordingly, we asked whether *Ty3* is under the control of Ndt80. If *Ty3* is a Ndt80 target, it would not be transcribed in meiotic cells deprived of Ndt80. Furthermore, *Ty3* transcription should be selectively activated upon ectopic Ndt80 activity. We found that cells in which *NDT80* is not induced – and are thus arrested in meiotic prophase – do not express *Ty3* mRNA (**Figure S2A, B**). Additionally, in meiotic cells where *NDT80* expression is delayed, *Ty3* transcription exhibits a corresponding delay. We observed that *Ty3* full-length transcripts accumulate from 15-30 min before metaphase I, and persist until exit from anaphase II (**Figure 2A, B**). These results imply that *Ty3* is a target of Ndt80.

In further support of this idea, *Ty3* is integrated downstream of two Ndt80 binding sites (79 bp and 269 bp) (**Figure 2C**). To investigate whether *Ty3* meiotic transcription activation is governed by its environment of integration rather than elements within its 5' LTR, we asked if *Ty3* is still transcribed in cells harboring a promoter-gene cassette (*HIS3MX*) between the 5' LTR and the first proximal Ndt80 binding site (**Figure S3A**). We found that *Ty3* was no longer transcribed when we separated it from its upstream genetic context (**Figure S3B**). To test whether Ndt80 directly activates *Ty3*, we mutated the two Ndt80 binding sites upstream of *Ty3* (CACAAA to AAAAAA) and assessed the effect of these mutations on meiotic *Ty3* transcription (**Figure 2C**). We found that point mutation of these sequences specifically abolished full-length meiotic *Ty3* transcription (**Figure 2D**). To assess whether Ndt80 binds upstream of *Ty3* during meiotic progression, we conducted a meiotic time course analysis of Ndt80 binding by ChIP-seq. We analyzed Ndt80 binding at 0, 3, 5, and 6 hours in meiosis. We chose these time points because Ndt80 levels are highest ~ 5-6 hours in meiosis (**Figure 2E**). In support of the hypothesis that *Ty3* is transcriptionally activated by Ndt80, we find that Ndt80 binds upstream of *Ty3* as meiosis progresses (**Figure 2F**). We conclude that *Ty3* co-opts a host regulatory circuit to coordinate its activation with meiotic division and we predict that other retroelements could have evolved a similar strategy to acquire germline-specific activation.

The Ndt80 protein sequence as well as its binding site is conserved among yeasts from *Saccharomyces* to *Candida* (Nocedal et al., 2017). We thus sought to determine whether *Ty3* control by Ndt80 is conserved among other *Saccharomyces*. We assessed the presence of Ndt80 binding sites within and upstream of full-length *Ty3* elements in seven *S. cerevisiae* and five *S. paradoxus* genomes for which all *Ty* elements have been mapped and annotated (Yue et al., 2017) (spanning approximately 5 million years of evolution (Shen et al., 2018)) (**Figure 3A**). Among twenty full-length *Ty3* elements, we found that thirteen harbor one or more Ndt80 binding sites within 1 kb upstream of their integration

sites, including five cases where the Ndt80 binding site is less than 250 bp upstream the integration site (**Figure 3A**). Within the 1 kb regions upstream of *Ty3* elements, we observed several that harbor multiple Ndt80 binding sites. In total, we observed nineteen Ndt80 binding sites within the 20 total kb which is significantly higher than what would be expected by chance (Z-score 2.7; $p < 0.01$).

Because Ndt80 binding sites are abundant (about 8,000/genome), we needed to ascertain whether the distance of a Ndt80 binding site from a locus is predictive of whether that locus is truly activated by Ndt80. Ndt80-responsive genes are well defined in SK1 meiosis (Chu et al., 1998). We first compared the enrichment of Ndt80 binding sites upstream of Ndt80 target genes and non-target genes, and found a peak of enrichment within the -50 to -250 bp region upstream of the transcription start sites (TSS) in target genes (**Figure 3B**). We next asked whether the association between *Ty3* elements and Ndt80 binding site resembles that of Ndt80 targets or non-targets. Because the small number of full-length *Ty3* found in the *Saccharomyces* mentioned above gave us limited statistical power, we combined full-length elements with *Ty3* solo-LTRs (n=498), which are the vestiges of *Ty3* integrations lost by homologous recombination between LTRs. We found that taken together, *Ty3* elements showed a significant enrichment of Ndt80 binding sites 200 bp upstream of their integration site ($p < 0.001$, **Figure 3B**). This result strongly supports the hypothesis that the co-opting of Ndt80 by *Ty3* elements is a recurring feature.

Ty3 translation is repressed specifically in meiosis

Ty3 has co-opted a meiotic control element to activate its transcription specifically during meiosis. We next sought to determine how yeast responds to protect its developing gametes from the potential threat of *Ty3* proliferation. Because *Ty3* copy number seems to be relatively low and stable in yeast strains (**Table S2**), we reasoned that yeast cells might have evolved a defense mechanism that acts post-transcriptionally. We first wanted to ascertain whether Gag3 protein is produced in meiosis. We found that Gag3 was produced in our positive control – exposure of *MAT*a SK1 haploid cells to α-factor mating pheromone (**Figure 4A**) – a condition in which full length *Ty3* RNA was shown to be both transcribed and translated in another lab strain via the transcription factor Ste12 (Bilanchone et al., 1993). Hence, we confirmed that *Ty3* is an active element in SK1. However, despite the presence of full-length *Ty3* mRNA in meiosis, no detectable Gag3 protein was produced (**Figure 4A**). The absence of Gag3 protein in meiosis could be due to a lack of translation or rapid protein degradation. To test the latter possibility, we inhibited proteasomal function in meiotic cells. We found that either genetic (*rpn6-1* (Isono et al., 2005)) or chemical inhibition (MG-132) of the proteasome did not result in Gag3 protein accumulation (**Figure S4A**). We concluded that the absence of Gag3 in meiosis is not due to

degradation by the proteasome. Our data instead support a model by which in response to *Ty3* transcription in meiosis, yeast cells respond by preventing translation of the mRNA thereby halting the retrotransposition cycle.

Because *Ty3* mRNA can be translated upon exposure of *MAT*a cells to α-factor pheromone, we suspected that translational repression of *Ty3* is specific to meiosis. To test this hypothesis, we ectopically expressed *NDT80* in haploid mitotic cells to drive *Ty3* transcription. In parallel, we depleted the mitotic repressor Sum1 which binds upstream of Ndt80 target genes to inhibit their inappropriate expression (Klutstein et al., 2010; Pierce et al., 2003; Winter, 2012). Selective depletion of Sum1 was achieved using the auxin-inducible degron system (Morawska and Ulrich, 2013). We found that when we expressed *NDT80* in mitotic cells either in the presence or absence of Sum1 (**Figure S4B**), *Ty3* was both transcribed and translated (**Figure 4B**). *Ty3* mRNA and protein levels were much higher when Sum1 was depleted. We also observed that upon *NDT80* activation in meiosis or mitosis, *Ty3* mRNA levels were similar, while translation occurred only in the mitotic context. In addition we observed that *Ty3* mRNA dimers, which are indicative of VLP assembly (Cristofari et al., 1999; Feng et al., 2000), form upon *NDT80* induction in mitosis but not meiosis (**Figure S4C**). We conclude that the mechanism by which yeast represses translation of *Ty3* mRNA is meiosis-specific. These data also provide additional support to the notion that this retrotransposon has co-opted the Sum1/Ndt80 regulon to restrict its expression to meiosis.

Meiotic *Ty3* repression is mediated by the translational repressor Rim4

We next sought to elucidate the mechanism of *Ty3* translational repression. Translational control of mRNA plays a central role in regulating gene expression during gametogenesis in virtually all sexual organisms (reviewed in (Kronja and Orr-Weaver, 2011)). In most organisms, transcription is shut off or limited during meiosis and regulation of gene expression relies on RNA-binding proteins that govern translation of previously transcribed mRNA. In *S. cerevisiae*, the RNA-binding protein Rim4 binds to and inhibits translation of mRNAs that encode protein products that are toxic when prematurely expressed but are necessary for late meiotic events (Berchowitz et al., 2013). We thus wanted to test whether repression of *Ty3* translation was mediated by Rim4. Because Rim4 is required for meiotic entry we designed a selectively degradable Rim4 using the auxin-inducible degron system (Morawska and Ulrich, 2013) such that we could deplete it just before activation of *NDT80*. We found that *Ty3* was translated upon premature Rim4 depletion (**Figure 5**). Rim4 must be assembled into an amyloid-like state in order to repress translation of its targets which requires the intrinsically disordered region (IDR) in its C-terminus (Berchowitz et al., 2015). We found that *rim4ΔIDR* mutants also translate *Ty3* (**Figure**

S5). While our genetic analyses do not allow us to distinguish whether Rim4 directly or indirectly regulates *Ty3* translation, we conclude that Rim4 amyloid-like repressors function in part to protect the germline from the proliferation of retrotransposons.

Mammalian *Gypsy*-derived genes are regulated by meiotic transcription factors

We next asked whether mammalian *Ty3/Gypsy*-like elements also exploit meiosis-specific transcription factors to activate during gametogenesis. In mammals most *Ty3/Gypsy* LTR-retrotransposon/retrovirus-derived elements no longer retain their retrotransposition capacity, and are classified based on whether *Gypsy*-internal sequences are present (28 loci in mouse and 693 loci in human contain *Gypsy*-internal sequences) (Campillos et al., 2006; Kojima, 2018). To test if any mammalian *Gypsy*-derived genes are switched on during meiosis, we analyzed RNA sequencing data from adult mouse testes (Soumillon et al., 2013). We found that several *Gypsy*-derived elements including those that contain Gag-like internal sequence (MamGyp-int) are transcribed in testes during the meiotic stage of spermatogenesis (spermatocytes) and in post-meiotic round spermatids (**Figure S6A**). When we analyzed uniquely mapping RNA sequencing reads of specific MamGyp-int loci, we found that two genes – *Moap1* and *Pnma1* – are highly upregulated in mouse meiotic spermatocytes (**Figure 6A**). Both *Moap1* and *Pnma1* are characterized as domesticated in mammals, and their open reading frames encode *Gypsy*-derived Gag-like proteins. Based on these analyses we propose that, analogous to *Ty3* regulation in yeast, the *Gypsy*-like sequences *Moap1* and *Pnma1* are being transcriptionally activated in male mouse meiosis. In eutherian mammals, there has been massive expansion of the *Pnma* gene family (15 genes in humans, 12 in mice (Campillos et al., 2006)). We wanted to test whether meiotic transcription of *Pnma* can be observed in marsupials which did not experience this expansion of *Pnma* genes and harbor only a single *Pnma* gene: *M-PNMA* (Kokošar and Kordiš, 2013). We analyzed tissue-specific RNA sequencing data from opossum (Lesch et al., 2016; Marin et al., 2017) and found that *M-PNMA* mRNA is highly and specifically upregulated in testes particularly in pachytene spermatocytes (**Figure S6B**). These data suggest that meiotic transcription of *Pnma* was either present in the common therian ancestor or has convergently evolved independently in both eutherians and marsupials.

We next wished to investigate if the transcriptional activation of *Gypsy*-derived elements in meiosis reflects the capture of element-external meiosis-specific transcription factor binding sites. Motivated by our findings in yeast, we focused our investigation on two master transcriptional regulators of meiosis: Stra8 and Mybl1 (also known as A-myb). Stra8 is required for meiotic initiation in mammals and promotes transcription of early meiotic genes (Anderson et al., 2008) whereas Mybl1 becomes active early in meiosis and is required for meiosis to progress through pachytene (Bolcun-Filas et al.,

2011). We assessed whether the meiotic transcription factors Stra8 and Mybl1 bind upstream of *Moap1* and/or *Pnma1* using ChIP-seq data from adult mouse testes (Kojima et al., 2019; Zhou et al., 2017). We found that both Mybl1 and Stra8 ChIP-seq peaks are present upstream of multiple *Moap1* TSSs (**Figure 6B, Figure S6C, D**). Similarly, a Mybl1 ChIP-seq peak overlaps the *Pnma1* TSS external to the MamGyp-int sequence (**Figure 6C, Figure S6C, D**).

If *Moap1* and *Pnma1* are under the direct control of Stra8 and Mybl1, developing gametes that do not express these transcription factors should not produce these transcripts. To test this prediction, we analyzed whether *Moap1* and *Pnma1* are expressed in preleptotene *Stra8*$^{+/-}$ and preleptotene *Stra8*$^{-/-}$ spermatocytes (Kojima et al., 2019) or in P14 *Mybl1*$^{+/-}$ and *Mybl1*$^{-/-}$ testes (Zhou et al., 2017). In concordance with the ChIP-seq analysis, *Moap1* transcript abundance is significantly reduced in the absence of *Stra8* (**Figure 6D**). In addition, both *Pnma1* and *Moap1* transcript abundance is reduced in the absence of *Mybl1* (**Figure 6E**). Taken together, our data support the hypothesis that *Gypsy* elements co-opt critical meiotic transcription factors to ensure their expression in gametogenesis and that this regulation exists from yeast to mammals.

Mammalian meiotic translational repressor proteins bind to *Gag*-containing mRNA

In mammals, the functional orthologs of Rim4 are the DAZ family of RNA-binding proteins (Berchowitz et al., 2015). DAZ family proteins act as regulators of translation and exhibit a similar organization to Rim4 in that they harbor N-terminal RRMs and a C-terminal prion-like domain (King et al., 2012). Furthermore, Dazl (DAZ-like) forms SDS-resistant amyloid-like assemblies specifically in mouse testes (Berchowitz et al., 2015). Thus, we asked whether meiotic *Gypsy*-derived RNAs might be regulated by DAZ family proteins. We analyzed Dazl CLIP data generated from adult mouse testes (Zagore et al., 2018) and observed clear enrichment peaks within the 3' UTRs of *Moap1* and *Pnma1* transcripts (**Figure 6B, C**). In addition, we analyzed DAZL-RNA complexes isolated by RIP in oocyte-containing human fetal ovaries (Rosario et al., 2017). We found that among human *Gypsy*-derived elements, the cognate human *MOAP1* and *PNMA1* transcripts are significantly enriched in DAZL immunoprecipitations (**Figure 6F, Figure S6E**). Of all the 802 different types of retrotransposon expressed in this tissue, only five were enriched in the DAZL RNA immunoprecipitations (**Figure S6F, G**). We propose that the physical interaction between DAZ family proteins and transcripts containing *Gypsy*-derived sequences exists in both mice and humans and in both male and female gametogenesis. Taken together, these data support an ancient association between amyloid-like RNA-binding assemblies and retrotransposon and retrotransposon-derived mRNA. We propose that this

association possibly represents a functional repurposing of the retrotransposon defense mechanism we observed in yeast.

DISCUSSION

In this study, we elucidate mechanisms underlying an evolutionary battlefront where retrotransposons attempt to proliferate in the germline and host organisms respond to defend the genomes of their progeny. *Ty3/Gypsy* retrotransposons in yeast and domesticated *Gypsy*-derived genes in mammals co-opt host master meiotic regulators to transcriptionally activate during gametogenesis. Based on these findings we propose that the integration site of a retrotransposon can encode the critical regulatory information that the element requires to activate specifically during gamete development. We further show that yeast cells utilize a meiosis-specific translational repressor to thwart further progress in the retrotransposon life cycle. Likewise, transcripts from domesticated *Ty3/Gypsy* elements in mammals are bound by a cognate translational regulator. In the yeast strain SK1, we find that meiotic cells efficiently repress translation of *Ty3* mRNA which very likely prevents the element from proliferating in this context. However, because the control of retrotransposons by meiotic transcription factors occurs frequently in yeast, we expect this activation strategy to be successful in other strains and other organisms. Future studies will be necessary to determine the extent to which meiotic activation and host translational repression of *Ty3/Gypsy* elements can be generalized across organisms.

Arkhipova and Meselson put forth the idea that one of the major forces driving the pervasive maintenance of meiosis and sex is to allow organisms to focus defense strategies against transposable elements to a subset of cells (i.e. the germline) that will provide the genetic material for generations to come (Arkhipova and Meselson, 2005). In multicellular organisms, it is of obvious benefit to the retrotransposon to direct activation to the germline with the aim to elude host defense mechanisms. Why does the *Ty3* retrotransposon activate only during the sexual cycle (meiosis and mating) in a unicellular organism such as yeast? In unicellular organisms, the entire organism is the germline and thus coordination of retrotransposon activation with meiosis may seem less obvious. Retrotransposon activation poses a resource cost on the cell (reviewed in (Bourque et al., 2018)). In rapidly proliferating cells, this cost could indeed translate into a fitness disadvantage. By restricting activation to meiosis and mating in yeast, *Ty3* remains latent, thus minimizing its fitness cost and focusing its efforts to proliferate in cells that are not cycling. Furthermore, linking retrotransposon proliferation to meiotic recombination i.e. mixis could be valuable for the element. Organisms can generate favorable allelic combinations via meiotic recombination. Retrotransposons could propagate into advantageous allelic combinations by activating during and post-recombination which could offset the fitness cost of an additional element. Lastly, the programmed double-strand breaks that initiate meiotic recombination could provide access points for retrotransposon cDNA.

The transcriptional activation of LTR-retrotransposons is often governed by regulatory sequences within the LTRs themselves. For example, the 5' LTR of *Ty1/Copia* contains binding sites for several transcriptional activators including Gcn4, Gcr1, Ste12, Tec1, and Tea1 and the repressor Mot3 (Servant et al., 2008). Likewise, the ability of *Ty3/Gypsy* to activate during mating (or upon α-factor exposure) relies on Ste12 binding within its 5' LTR (Bilanchone et al., 1993). In the situation described here however, *Ty3* utilizes regulatory sequences upstream of its integration site. What selective pressures then would drive *Gypsy*-like elements to utilize external regulatory sites to activate during meiosis? We propose that there may be some advantage to decouple meiotic activation from the intrinsic properties of the element. Meiosis-specific genes are repressed during vegetative/somatic growth. As we mentioned above, in yeast the Ndt80 binding site is also recognized by the repressor Sum1 (Klutstein et al., 2010; Pierce et al., 2003). If this sequence was harbored in the 5' LTR, the element could be condemned to a single strategy by virtue of the presence of Sum1 in non-meiotic contexts. By utilizing external regulatory elements, the element can avoid intrinsic repressor binding sites while gaining the flexibility to utilize other transcription activators that may be advantageous in other selective contexts.

As illustrated by decades of previous work, the study of *Ty* elements is a powerful model for the discovery and elucidation of host mechanisms that restrict retrotransposition (Maxwell and Curcio, 2007). Genetic screens designed to identify factors that influence *Ty1* (Griffith et al., 2003; Scholes et al., 2001) and *Ty3* (Aye et al., 2004; Irwin et al., 2005) retrotransposition have shown that RNA processing factors can positively and negatively influence *Ty* retrotransposition. Three RNA processing factors suppress both *Ty1* and *Ty3* retrotransposition: The DExH-box RNA helicase Dbp3, The ribosomal protein Rpl6A, and the lariat debranching enzyme Dbr1. Studies motivated in part from these screens have identified that mRNA processing bodies (P-bodies) (Beliakova-Bethell et al., 2006) and nucleoporins (Rowley et al., 2018) play important roles in the life cycle of *Ty3* elements. Here, we show that host repression of *Ty3* is either directly or indirectly carried out by amyloid-like assemblies of the RNA-binding protein Rim4 – *rim4⊿IDR* mutants that fail to assemble also fail to repress *Ty3* translation. It will be exciting in future studies to assess whether and how Rim4 assemblies interact with these factors to defend the host genome against retrotransposon proliferation.

Rim4 binds to and represses translation of numerous mRNAs that encode proteins required for late meiotic events. While many of these targets are translated precisely at meiosis II onset, several others are translated later (Berchowitz et al., 2013; Brar et al., 2012) and apparently some, such as *Ty3*, are seemingly never translated. We hypothesize that the fate of Rim4 targets is dictated by interaction with other factors. This hypothesis is consistent with the developmentally-regulated clearance of Rim4 multimeric assemblies at meiosis II onset (Carpenter et al., 2018). Targets that are

translated significantly after meiosis II onset likely interact with the RNA-binding proteins Pes4 and Mip6 (Jin et al., 2017) and we speculate that the terminal repression that we observe for *Ty3* is carried out by a factor unknown to us.

To escape Rim4-mediated translational repression, *Ty3* could take the advantage of a particular feature of the meiotic stage at which it is expressed. Prior to meiotic prophase exit, cells can return to a mitotic cycle if nutrients are sensed by the cell in a process known as return to growth which is a common event in the life cycle of wild yeast (Brion et al., 2017; Tsuchiya et al., 2014). *Ty3* mRNA accumulates 15-30 minutes before the meiotic commitment point. Upon return to growth, Rim4-mediated translational control is relieved (Jin et al., 2017) and therefore *Ty3* would recover the ability to propagate in a post-mixis environment. Similarly, if *Ty3* mRNA persists until the end of gametogenesis and into spores, germination would likely provide a permissive environment for *Ty3* propagation. This strategy would be analogous to what is observed in LINE-1 elements which are expressed during mouse gametogenesis and then only re-integrate after fertilization during early embryonic development (Kano et al., 2009).

While the proliferation of *Ty3/Gypsy* elements is often deleterious it is possible that their evolutionary cost is offset by providing an activity or function that is beneficial to the host (Cosby et al., 2019). Our preliminary results suggest that *Ty3* deletion mutants do not exhibit a detectable defect (or advantage) in any aspect of gametogenesis including meiosis, spore formation, and/or spore viability. However, we speculate mutations in other *Ty* elements could be different in this regard. One exciting speculation is that by integrating downstream of meiosis-specific regulatory elements, a new coding sequence is now readily available to be domesticated for a meiosis-specific function. Similarly, the interaction of retrotransposons with regulatory RNA-binding proteins could connect the evolving gene to additional regulatory pathways. Retrotransposons are ripe for domestication because they encode several proteins with diverse and useful domains (Volff, 2006). Possible examples of meiotic genes evolving from *Gypsy* sequences include the mammalian *Gypsy*-like elements *Moap1* and *Pnma1* which do not represent active retrotransposons and are likely domesticated. We observe meiotic transcriptional activation of *Pnma* genes in mouse, human, and opossum and while meiosis-specific activation of *Gypsy*-like elements is unlikely to be generalizable among all copies of these elements within a species, it appears to be generalizable to some degree among species. Remarkably, the single *Pnma* gene (*M-PNMA*) in opossum is highly upregulated in pachytene spermatocytes. Whether this represents the ancestral expression pattern of *Pnma* or convergent evolution, we speculate that meiotic activation of *Pnma* is providing some benefit to the organism and is being selected for. Because *Pnma* is inactive for retrotransposition, we propose that during the time when *Gypsy* elements were still retrotranspositionally active and co-opting meiotic transcription factors for their own benefit, they

acquired beneficial functions in the host meiotic cells. It is exciting to us that the regulatory circuitry established during the evolutionary battle between host and retrotransposon could also give direction as to how and when the emerging gene will function. It will be important to investigate the emerging roles of these elements and how they are repurposing retrotransposon regulatory mechanisms in the process of acquiring functions and evolving into new genes.

We propose that the co-opting of meiosis-specific transcription factors by retrotransposons represents an ancient strategy to coordinate retrotransposition with germline development. Correspondingly, translational repression of retrotransposons by host RNA-binding proteins could also be an ancient and preserved feature of meiosis. We can add this mechanism to the elaborate repertoire of retrotransposon defense systems such as piRNA, DNA methylation, and heterochromatic DNA condensation. It will be interesting to assess whether other assembly-forming RNA-binding proteins intervene in the life cycles of other retrotransposons in other organisms.

ACKNOWLEDGMENTS

We would like to thank Virginia Bilanchone and Suzanne Sandmeyer for providing the anti-Ty3 VLP crude serum, Kayla Carpenter for RNA sequencing prep, and S. Grace Herod for the *his3::pRIM4-OsTIR1::His3MX6* construct. We would like to thank Albert Serra Cardona and Zhiguo Zhang for help with Ndt80 ChIP. We would also like to thank Stephen Goff and members of the Berchowitz lab for valuable discussions and Jonathan Dworkin, Diana Ottoz, and Tanguy Lucas for critical reading of the manuscript. This research is supported by The Schaefer Research Scholars Program, The Hirschl Family Trust, NIH grant R35 GM124633-01 to L.E.B., MRC University Unit grant MC_UU_00007/6 to I.R.A., Agence Nationale de la Recherche grant ANR-16-CE12-0019 to G.L. and National Institutes of Health DP2 AG055946-1250 01 to EÜ. Finally, we would like to thank Harmit Malik who suggested an idea to L.E.B. that provided the motivation to begin this project.

AUTHOR CONTRIBUTIONS

L.E.B. and R.L. conceived of the study. L.E.B. and R.L. designed the molecular biology and yeast computational experiments. I.R.A. designed and analyzed the mammalian computational biology experiments. R.L. led the experimental procedures. R.L., A.D., G.D., S.B., H.A., E.U., A.H. and L.E.B. built strains, performed experiments, and analyzed the data. G.L., J.-X.Y., and M.D.C. screened the wild yeast strains for sporulation efficiency. L.E.B. and R.L. wrote the paper with input from all authors. The manuscript was edited by I.R.A, E.U., and G.L.

DECLARATION OF INTERESTS

The authors declare no competing interests**.**

MAIN FIGURE TITLES AND LEGENDS

Figure 1: *Ty3* expression is coordinated with meiotic progression

(A) Diagram of the SK1 *Ty3* element DNA locus, full-length mRNA, and two polyproteins Gag3 (precursor of CA-capsid SP-spacer and NC-nucleocapsid proteins) and Gag3-Pol3 (precursor of the aforementioned proteins and of PR-protease, RT-RH-reverse transcriptase – RnaseH and IN-integrase proteins). Colored lines indicate the positions of the Northern probes used in this study: *Ty3* probe (maroon), CA probe (orange), PR probe (yellow), RT probe (green), IN probe (blue).
(B) $\log_2$ tag density of polyA-RNAseq reads of *Ty3* locus from synchronized meiotic cells (Crick strand top). Cells harboring *NDT80-IN* (*NDT80* inducible strain B119) were sporulated at 30º C. Shown are the time points 0, 3, 6, 7, 8, and 9 h post transfer to sporulation medium. At 6 h when cells had arrested in G2 due to the lack of Ndt80 meiotic transcription factor, they were released from the block by addition of 1 µM β-estradiol (biological replicates = 2).
(C, D) Full-length *Ty3* mRNA is expressed in meiosis. Sporulation was induced in wild type diploid strain (B47, purple) and in *ty3*Δ diploid strain (B837, gold). **(C)** *Ty3* mRNA and *rRNA* (loading control) levels are shown (S = pre-meiotic DNA replication, G2 = meiotic prophase, MI = first meiotic division, MII = second meiotic division). Full-length *Ty3* mRNA (5 kb) is indicated by a black arrow. Empty arrowheads indicate 18S and 25S *rRNA* (1.8 kb, 3.4 kb), both reported on the probed blot and serve as size markers. **(D)** Kinetics of meiotic progression was determined via DAPI nuclear staining. Shown are representative results of ≥ 5 biological replicates.
(E-G) *Ty3* is activated during meiosis in wild *S. cerevisiae*. Wild type SK1 (B47, purple) and wild European strain OS673 (green, described in (Peter et al., 2018)) were induced to sporulate as in C. **(E)** *Ty3* mRNA and *rRNA* levels are shown. **(F)** The number of *Ty* elements in SK1 and OS673 are shown. **(G)** Kinetics of meiotic progression determined by DAPI nuclear staining (biological replicates = 2).

Figure 2: *Ty3* exploits binding sites of a meiotic transcription factor from the integration environment

(A, B) *Ty3* expression is controlled by Ndt80. **(A)** Sporulation was induced in parallel in wild type (B47, purple), and in *NDT80-IN* (B48, blue, released from the G2 block at 6 h). *Ty3* mRNA and *rRNA* levels are shown. Asterisk indicates a degraded RNA sample, which is excluded from the quantification shown in B. **(B)** Solid lines indicate quantification of RNA levels from A, dashed lines indicate kinetics of

meiotic divisions analyzed by tubulin immunofluorescence (quantification of cells containing meiotic spindles). Shown are representative results of ≥ 5 biological replicates.
(C, D) *Ty3* transcription is directly activated from Ndt80 binding sites upstream of the integration site. Diagram of endogenous and mutated *Ty3* upstream context. **(C)** Blue triangles indicate Ndt80 binding sites (CACAAA) and yellow triangles indicated mutated binding sites (AAAAAA) (-79 and -269 bp upstream of *Ty3*). **(D)** Sporulation was induced in *NDT80-IN* strains containing the wild type *Ty3* Ndt80 binding sites (B1864, blue), or with mutated Ndt80 binding sites (B1885, yellow) as in A (in both strains, a *kanMX* marker was inserted 353 bp upstream the *Ty3* 5' LTR). *Ty3* mRNA and *rRNA* levels are shown. Shown are representative results of 2 biological replicates.
(E, F) Ndt80 binds directly upstream of *Ty3* integration sites as meiosis progresses. Sporulation was induced in wild type diploid strain (B47 no tag) and in *NDT80-3V5* diploid strain (B1674). Shown are the time points 0, 3, 5, 6 h post-transfer to sporulation medium. **(C)** Analysis of Ndt80 protein expression. Ndt80 (tagged with 3V5) and Pgk1 (loading control) protein levels are shown. Migration of molecular size standards is indicated on right as kDa values. **(D)** Browser tracks showing Ndt80-3V5 ChIP-seq peaks (blue bars). *Ty3* (left) and *NDT80* (right, positive control) loci are shown.

Figure 3: Integration of *Ty3* downstream of Ndt80 is a recurring phenomenon

(A) Left: Phylogenetic relationships among seven *S. cerevisiae* (*S. c.*) strains and five *S. paradoxus* (*S. p.*) strains (modified from (Yue et al., 2017)), along with their respective number of full-length *Ty3* elements (total 20). Right: 2-kb window map of 1000 bp upstream of full-length *Ty3* elements with Ndt80 binding sites (CACAAA) indicated as blue triangles. Ndt80 binding sites are significantly enriched in this region (determined by Z-test statistic of 100 randomized simulations; Z-score 2.7; $p < 0.01$) **(B)** Left: 260 SK1 genes were identified as Ndt80 target genes (Chu et al., 1998), and 5291 as non-target genes. Within the 13 *S.c.* and *S.p.* strains analyzed above there are 518 *Ty3* elements (20 full-length and 498 solo-LTRs). Right: Comparison of the distribution of Ndt80 binding sites in the region 500 bp upstream of the TSS among target genes (teal), non-target genes (grey), and *Ty3* elements (blue). Statistical significance was determined by bootstrap analysis ($p < 0.001$ at the -200 position).

Figure 4: *Ty3* is post-transcriptionally repressed in meiosis

(A) Gag3 protein encoded by *Ty3* is not detectable during meiosis. Sporulation was induced in *NDT80-IN* (B48) as in 2A. *MAT*a wild type (B1) and *ty3*Δ (B827) haploid strains were exposed to α-factor (0, 0.5μM, 10μM) to induce *Ty3* activation. Left: *Ty3* mRNA (black arrow) and *rRNA* (white arrows) levels,

and Gag3 (and its processed forms CA-SP, CA) and Pgk1 (loading control) protein levels are shown. Migration of molecular size standards is indicated on right as kDa values. Right: Quantification of *Ty3* full-length RNA (maroon) and Gag3 protein (green) normalized over their respective loading controls. Shown are representative results of ≥ 5 biological replicates.

(B) Post-transcriptional repression of Gag3 is specific to meiosis. To express *Ty3* in both meiosis and mitosis, we expressed *NDT80* in sporulating diploid cells (wild type B48, *ty3*Δ B839) and in haploid mitotically dividing cells with and without the Sum1 transcriptional repressor (wild type B477, Sum1-deg B829, and *ty3*Δ B827). *Ty3* mRNA (black arrow) and *rRNA* (white arrows) levels and Gag3 and Pgk1 (loading control) protein levels and quantification are shown, as in A. Asterisks show unspecific bands (e.g. band in α-VLP present in *Ty3*Δ - see also Figure S3B). Shown are representative results of 5 biological replicates.

Figure 5: *Ty3* is translationally repressed by the RNA-binding protein Rim4

Gag3 protein accumulates upon Rim4 depletion in meiosis. Meiosis was induced in three *NDT80-IN* diploid strains: wild type (B48), Rim4-deg (B1022, Rim4-degron fusion strain, induced by auxin addition to 1 mM at t = 5 h), and *ty3*Δ (B389). Meiotic cells were released from the G2 block by addition of 1 µM β-estradiol at 6 h. Mitotic samples were collected from the experiment shown in 3B and Figure S3B. *Ty3* mRNA (black arrow) and *rRNA* (white arrows) levels and Gag3, Rim4 (Rim4-deg is tagged with FLAG, wild type Rim4 is tagged with 3V5 in the first strain, and not tagged in the remaining strains), and Pgk1 (loading control) protein levels. Migration of molecular size standards is indicated on right as kDa values. Quantification of *Ty3* mRNA and Gag3 protein relatively to their respective loading controls are shown. Asterisks show unspecific bands (e.g. band in α-VLP present in *ty3*Δ - see also Figure S3B). Shown are representative results of 4 biological replicates.

Figure 6: Mammalian *Gypsy*-derived genes are activated by meiotic transcription factors and regulated by meiotic RNA-binding proteins

(A) Analysis of uniquely mapping MamGyp-int RNAseq reads for MamGyp-int loci expressed during spermatogenesis in adult mouse testes. biological replicates = 3 for each stage.

(B, C) Browser tracks showing mouse testis Stra8-FLAG ChIP-seq peaks (orange bars, MACS2 q < 0.05), mouse testis Stra8-FLAG ChIP reads (orange line plot, fold change in ChIP relative to input, data from wild-type animals subtracted as background), mouse testis Mybl1 ChIP-seq peaks (blue bars, MACS2 q < 0.05), mouse testis Mybl1 ChIP reads (blue line plot, fold change relative to input), mouse

testis Dazl CLIP clusters (green bars, biologically reproducible CLIP clusters), mouse testis Dazl CLIP (green line plot, number of CLIP tags), mouse spermatocyte RNA-seq (black histogram, counts per million mapped reads), Gencode VM18 gene models encompassing (B) *Moap1*, or (C) *Pnma1* (navy rectangles), and the genomic location of *Gypsy*-derived sequences (maroon rectangles).
(D) Expression of *Moap1* and *Pnma1* in *Stra8*$^{-/-}$ preleptotene mouse spermatocyte RNAseq data. CPM, counts per million mapped reads (biological replicates = 2 for *Stra8*$^{+/-}$ spermatocytes and = 3 for *Stra8*$^{-/-}$ spermatocytes).
(E) Expression of *Moap1* and *Pnma1* in P14 *Mybl1*$^{-/-}$ mouse testis RNAseq data (biological replicates = 3).
(F) Analysis of MamGyp-int containing transcripts from *MOAP1* and *PNMA1* in anti-DAZL RIP from human foetal ovaries (biological replicates = 3).

Asterisks indicate $p < 0.05$ as determined by Student's t-test.

MAIN TABLES AND LEGENDS

N/A.

STAR METHODS

RESOURCE AVAILABILITY

Lead Contact

Further information and requests for resources and reagents should be directed to and will be fulfilled by the Lead Contact, Luke E. Berchowitz (leb2210@cumc.columbia.edu).

Materials Availability

All strains and reagents used in this study are available upon request.

Data and Code Availability

The accession number for the RNA sequencing and ChIP sequencing dataset generated during this study is EBI ENA / NCBI BioProject: PRJNA669383 (https://www.ncbi.nlm.nih.gov/bioproject/?term=PRJNA669383 ; https://www.ebi.ac.uk/ena/browser/view/PRJNA669383).
Custom code and algorithms are available upon request.

EXPERIMENTAL MODEL AND SUBJECT DETAILS

Yeast strains and constructs

Lab strains are described in Supplementary **Table S1**, and wild strains in Supplementary **Table S2**. Strains were constructed by crossing and/or using the PCR-based method described in (Longtine et al., 1998) using the SK1 genome reference and annotation from (Yue et al., 2017). PCR and fusion PCR involved templates pFA6a-kanMX6 and pFA6a-His3MX6 (Longtine et al., 1998) and pUB976 (Sawyer et al., 2019). Seamless deletion of *Ty3* was introduced by pop-in pop-out procedure as described in (Storici et al., 2001), using pRG206MX (Gnügge, 2015) as template to delete *Ty3* at the pop-in step. The origins of all constructs are listed in the key resources table (this study, or (Benjamin et al., 2003; Berchowitz et al., 2013, 2015; Carlile and Amon, 2008; Carpenter et al., 2018; Torres et al., 2007)).

METHOD DETAILS

Yeast growth and sporulation conditions

All yeast strains were grown at 30° C. For sporulation of lab strains, strains were pulled from -80º C stock and grown on YPG (3% glycerol) plates overnight, were then transferred to YPD 4% (YPD + 4% glucose) plates for 24 h, were then grown to saturation in YPD for 24 h, diluted in BYTA (1% yeast extract, 2% tryptone, 1% potassium acetate, 50 mM potassium pthalate) to OD_{600} = 0.3 and grown overnight. Cells were washed with water, resuspended in sporulation medium (0.3% potassium acetate [pH 7.0], 0.02% raffinose) to OD_{600} = 1.8. Following inoculation into sporulation medium, cells were incubated with vigorous shaking (t = 0 h). For Rim4-deg strain, at t = 5 h, auxin (indole-3-acetic acid, Sigma) was added to a final concentration of 1 mM in order to induce degradation of Rim4. For *pdr5* mutant strain, proteasome inhibitor MG-132 was added at 6 h to 50 µM. For *NDT80-IN* (Benjamin et al., 2003) strains, at t = 6 h, β-estradiol was added to a final concentration of 1 µM (5 mM stock in ethanol, Sigma E2758-1G) to induce expression of *NDT80* from the *GAL1-10* promoter by activating the Gal4.ER fusion protein. For sporulation of wild strains, the procedure was essentially the same with the exception that if tetrads were already observed after overnight on YPG plates, they were pulled again from -80º C directly on YPD 4%, and the protocol was continued from there. Time points were taken for Western and Northern blot analysis and immunofluorescence/DAPI as indicated.

For mitotic Ndt80/Sum1 experiments, strains were grown overnight in YPG (glucose in YPD would inhibit the *GAL1-10* promoter driving *NDT80*) and diluted to OD_{600}= 0.3. Following transfer to fresh YPG medium, cells were incubated with vigorous shaking for 3 h. Then auxin (indole-3-acetic acid, Sigma) was added (t = 0h) to a final concentration of 1 mM in order to induce degradation of Sum1. After 1 hour, β-estradiol was added to a final concentration of 1 µM (5 mM stock in ethanol, Sigma E2758-1G) to induce expression of *NDT80* from the *GAL1-10* promoter by activating the Gal4.ER fusion protein. Time points were taken for Western and Northern blot analysis as indicated (collected volumes were adjusted to the OD_{600} at each time point).

For pheromone exposure experiments, strains were grown overnight in YPD and diluted to OD_{600}= 0.2. Following transfer to fresh YPD medium, cells were incubated with vigorous shaking for 3 h. Cells were pelleted and resuspended at an OD_{600} of 0.36 (t = 0 h), then α-factor (Genscript) was added to a final concentration of 0.8µg/mL (0.5 µM, “+”) or 16µg/mL (10 µM, “++”) in order to induce *Ty3* activation. Time points were taken for Western and Northern blot analysis as indicated (collected volumes were adjusted to the OD_{600} at each time point).

Meiotic progression analysis

Cells were fixed in 3.7% formaldehyde. For analysis of nuclear divisions and spindle visualization, indirect immunofluorescence was performed as in (Carpenter et al., 2018) with minor modifications. To visualize spindles, we used rat anti-tubulin antibody (Bio-Rad) at a dilution of 1:200, and anti-rat-FITC antibody (Invitrogen) at a dilution of 1:200. Immunofluorescence samples were mounted in ProlongGold (Invitrogen) that included DAPI. Acquisition of images was conducted using a DeltaVision microscope (GE Healthcare). Spindle morphologies (n = 100 cells per time point) were classified as in (Lee and Amon, 2001). Briefly, Metaphase I cells were defined as cells with a single DAPI mass spanned by a short, thick, bipolar, meiotic spindle. Anaphase I cells were defined as cells with two distinct (though not always separated) DAPI masses, and a single long spindle that spans both DAPI masses. Metaphase II cells were defined as cells with two separate DAPI masses with each spanned by a bipolar, short, thick, meiotic spindle. Anaphase II cells were defined as cells with four distinct (though not always separated) DAPI masses with two long spindles. Then, these four categories of cells were grouped under the label “cells in meiotic divisions”.

For analysis of nuclear divisions only, cells were washed once with 100 mM phosphate, 1.2 M sorbitol buffer [pH 7.5], permeabilized with 1% Triton X-100 and stained with 0.05 µg/ml DAPI.

Northern blot analysis

Samples were prepared by snap freezing the pellet of 7.2 OD_{600} units of cells, and total RNA was isolated using a (400 µL: 400 µL) mixture of TES buffer (10 mM Tris [pH7.5], 10 mM EDTA, 0.5% SDS) and acid phenol: chloroform 5: 1 (Ambion) with zirconia/silica beads (BioSpec) while shaking at 1400 rpm (Thermomixer, Eppendorf) at 65°C for 30 min. After centrifugation at 16,000 g for 5 min, the supernatant was ethanol precipitated at -20°C overnight (1 ml 100% ethanol and 40 µl 3M sodium acetate [pH 5.5]), centrifugated at 16,000 g for 20 min, washed in 80% ethanol, dried, and resuspended in DEPC–treated water. For wild strains, RNA extraction required two chloroform purification. 5 µg of RNA was denatured at 55°C for 15 min in 50% formamide, 18.3% formaldehyde, and 5% MOPS and was resolved on a denaturing agarose gel (1.9% agarose, 3.7% formaldehyde, 1x MOPS buffer) for 2.5 hours at 80 V. RNA was transferred to a Hybond-N+ membrane (GE Healthcare) by capillary transfer in 10x SSC (1.5 M NaCl, 0.15 M trisodium citrate dihydrate, [pH 7]). The membrane was stained with methylene blue, incubated in hybridization Buffer (0.25 M Na-Phosphate [pH 7.2], 0.25 M NaCl, 1 mM EDTA, 7% SDS, and 5% dextran sulfate) at 65°C and probed with ^{32}P–labeled PCR products prepared via Amersham Megaprime DNA labeling kit (GE Healthcare) and Illustra ProbeQuant columns (GE

Healthcare), transferred to a phosphor screen, and imaged on a Typhoon Trio variable mode imager (Amersham).

To observe *Ty3* dimers we conducted semi-denaturing Northern blot analysis (adapted from (Nymark-McMahon et al., 2002)). Briefly, the procedure is as above except we omitted formamide in the denaturing mix and incubated 15 minutes at 30°C.

Yeast RNA sequencing and sequencing analysis

Briefly, poly-A pull-down was used to enrich mRNAs from total RNA samples and proceed on library preparation by using Illumina TruSeq RNA prep kit. Libraries were sequenced using single-end sequencing (100 bp) in multiplex using Illumina HiSeq4000 at Columbia Genome Center. RTA (Illumina) was used for base calling and bcl2fastq2 (version 2.17) for converting BCL to fastq format, coupled with adaptor trimming. Sequencing reads were mapped onto SK1 genome reference (Yue et al., 2017) using STAR (Dobin et al., 2013) with the following parameters: Multiple alignments allowed: 500 (takes into account the number solo-LTR loci in the genome); Multiple alignment retained: 1; Order of multiple alignments: Random (--outFilterMultimapNmax 500 --outSAMmultNmax 1 --outMultimapperOrder Random --outFilterScoreMinOverLread 0.3 --outFilterMatchNminOverLread 0.1 --seedSearchStartLmax 20 --seedSearchStartLmaxOverLread 0.2) while other parameters were set to defaults. Reads count were scaled by CPM (count per millions) and visualized using Ving software (Descrimes et al., 2015).

Immunoblot analysis

The pellet of 7.2 OD_{600} units of cells was resuspended in 5% TCA, incubated overnight at 4° C, washed with acetone, and dried. Cells were broken using 50 µl acid-washed glass beads (Sigma), 100 µl lysis Buffer (10 mM Tris-HCl [pH 11], 1 mM EDTA [pH 8], 2.75 mM DTT, Halt protease inhibitors (Thermo Fisher)), and a 45 sec process in a FastPrep-24 (MP Biomedicals) at max speed. 50 µL Loading Buffer (9% SDS, 0.75 mM Bromophenol blue, 187.5 mM Tris-HCl [pH 6.8], 30% glycerol, and 810 mM β-mercaptoethanol) was added, samples were heated at 100°C for 5 mins, and centrifuged 5 mins at 20,000 g. Polyacrylamide gels (precast 10% Criterion TGX Precast Midi Protein Gel 26 wells, Bio-Rad) were run on a midi gel system (Criterion Vertical Electrophoresis Cell, Bio-Rad) with SDS Running Buffer (190 mM glycine, 25 mM Trizma base, 3.5 mM, 1% SDS), with 4 µl sample per well. They were transferred using a semi-dry transfer apparatus (Trans-Blot Turbo Transfer System, Bio-Rad) to a

nitrocellulose membrane (Trans-blot turbo transfer kits – Nitrocellulose, Bio-Rad), and stained in Ponceau.

α-VLP antibody was purified from α-VLP (Ty3) crude serum (gift from Sandmeyer lab), using Gag3 protein produced from pLZL2422 (Larsen et al., 2008) coupled to an AminoLink column (Thermo).

Antibodies were prepared in 1X TBST with 1% milk 1% BSA. Primary antibodies were used at the following concentrations: α-VLP (purified from α-VLP (Ty3) crude serum, gift from Sandmeyer lab) 0.1ug/mL, α-HA.11 1: 1,000 (BioLegend), α-V5 1: 2,000 (Invitrogen), α-FLAG (Sigma) 1: 800, α-Pgk1 1: 20,000 (Novex). α-mouse or α-rabbit HRP-conjugated secondary antibodies (GE Healthcare) were used.

Ndt80 ChIP-seq

NDT80-3V5 and no tag control cells were sporulated at 30° C. Cells were fixed in 1% formaldehyde for 15 minutes at room temperature and quenched with 0.1 M glycine (final concentration). Samples were prepared by snap freezing the pellet of 20 OD_{600} units of cells. Cells were resuspended in 0.4 ml lysis buffer (50 mM HEPES/KOH pH [7.5], 140 mM NaCl, 1 mM EDTA, 1% Triton-X, 0.1 % Na-deoxycholate, 1 mM PMSF) lysed with zirconia/silica beads (BioSpec) in a FastPrep homogenizer. The homogenate was centrifuged at 2,500 rpm for 1 minute and the supernatant was discarded. The pellet was resuspended in 0.25 ml lysis buffer and sonicated (15 sec on, 30 sec off, 10 cycles). Lysate was centrifuged at 10,000 g for 5 minutes at 4° C and supernatant was transferred to a new tube. 50 µL was taken for DNA input sample and the remaining sample was processed for ChIP.

Ndt80-DNA complexes were immunopurified using anti V5 agarose beads (Sigma) for 1 h at 4° C. Beads were washed and crosslinks were reversed using Chelex resin (Bio-Rad). Elution was carried out by boiling samples for 10 minutes followed by Proteinase K digestion (1 mg/ml 30 min at 55° C). Beads were boiled again for 10 minutes and the eluate was collected and purified/concentrated using a Qiagene Minelute kit. Sequencing libraries were prepared from the eluate using an Accel-NGS 1S plus (Swift Biosciences) per the manufacturer's protocol. Libraries were sequenced using paired-end sequencing (2x100 bp) in multiplex using NextSeq 550.

QUANTIFICATION AND STATISTICAL ANALYSIS

Immunoblot and Northern blot were quantified using FIJI software (Schindelin et al., 2012). Signal intensity was normalized to a loading control (Pgk1 for immunoblots, 25S rRNA for Northern blots).

Values were multiplied by an arbitrary scaling factor, which was held constant within each figure panel for each technique. Statistical significance was determined by Student's T-test or Z-test statistic as indicated. Number of biological replicates is indicated in figure legends where applicable.

Statistical analysis for Ndt80 binding site enrichment upstream *Ty3* insertions

Data analysis was performed using the R project for statistical computing version 3.6.1 (https://www.r-project.org) and RStudio version 1.1.383 (https://www.rstudio.com), utilizing the following packages: dplyr, tidyr, stringr, ggplot2, plotly, tools, boot, Biostrings, GenomicRanges, janitor, seqinr, BiocManager, TFBSTools. Briefly, yeast genomes were downloaded from (Yue et al., 2017) and Ndt80 binding sites (defined as CACAAA by (Nocedal et al., 2017)) were identified. Then the positions of Ndt80 binding site upstream *Ty3* elements (full-length or solo-LTRs) were recorded. For Ndt80 target genes and non-target genes in SK1, the same process was applied, using the SK1 reference genome and annotation from (Nocedal et al., 2017). For bootstrap, the R function sample_n was used to take samples with replacements. Then the data was visualized using 50 bp long non-overlapping bins. We used the distribution of outlier boundaries for each bootstrap experiment to identify region of significant difference in Ndt80 binding site enrichment.

Analysis of yeast ChIPseq data

Reads were trimmed of their adaptors using cutadapt (Martin, 2011) and were aligned to the *S. cerevisiae* SK1 genome (Yue et al., 2017) using Bowtie2 version 2.3.4 (Langmead and Salzberg, 2012). Alignments were filtered using samtools v1.6 (Li et al., 2009) (samtools view -f 2 -F 1804 -q 30), and PCR duplicates were filtered out using Picard tool MarkDuplicates v2.23.3 (Broad Institute). Deeptools bamcoverage (Ramírez et al., 2016) was used to generate a coverage track of number of reads per bp after reads were extended to their mates, to reflect the actual fragment length. Coverage was then normalized using a script detailed in (De Muyt et al., 2018): upon the assumptions that for a transcription factor, peaks are expected to be narrow, they are expected to fall in the top outliers of the coverage distribution, while the background regions are expected to fall in the bulk of the distribution, between Q1-1.5IQR and Q3+1.5IQR. Hence, for untagged immunoprecipitate (UIP), the coverage was divided by the average read count in non-null and non-outlier positions, while for tagged immunoprecipitate (IP), the coverage was divided by the average read count in non-null and non-outlier positions and multiplied by the average read count of the same set of positions in the normalized UIP. Normalized profiles were used for peak detection using bpeaks v1.2 (Merhej et al., 2014) using as

thresholds: T1: IP>($Q3_{UIP}$ + 1.5IQR_{UIP})*mean(IP), T2: UIP>($Q1_{UIP}$ − 1.5IQR_{UIP})*mean(UIP), T3: log2FC>0.5, and T4: ((log2(IP)+1)+(log2(control)+1))/2>0. For visualization on IGV (Thorvaldsdóttir et al., 2013), normalized UIP profiles were subtracted to their corresponding normalized IP profiles using Deeptools bigwigCompare (Ramírez et al., 2016).

Analysis of mammalian RNAseq data (mouse, opossum)

RNAseq from enriched populations of adult mouse testicular cell types (Soumillon et al., 2013) was downloaded from EBI ENA (https://www.ebi.ac.uk/ena, accession PRJNA187158). Reads were trimmed to remove adapter sequences (--stringency 5 --length 20) using TrimGalore 0.4.1 (https://github.com/FelixKrueger/TrimGalore) then aligned to the mm10 reference assembly of the mouse genome with Tophat v2.1.0 (Kim et al., 2013) (command line options -g 1 --no-coverage-search --b2-sensitive) using the GencodeBasic VM18 transcriptome as a transcriptome index (Frankish et al., 2019). Accepted hits from Tophat were filtered with samtools v1.6 (Li et al., 2009) to remove unmapped reads and non-primary alignments. For locus-specific analysis, uniquely mapping reads were selected by removing reads with a quality score below 5. Reads overlapping Repeatmasker-annotated loci in the mouse genome were counted for each repeat locus, and aggregated at the level of the repeat name (repName). EdgeR (Robinson et al., 2010) was then used to normalize the counts per million mapped fragments in each sample using trimmed means. CPMs were converted to fragments per kilobase of transcript per million mapped reads (FPKM) by dividing CPM by the length of the repeat locus for locus-specific analysis, or by the mean length of repeat loci annotated with that repeat name for repName-level analysis.

RNAseq for P14 *Mybl1* testes (Zhou et al., 2017) and *Stra8* preleptotene spermatocytes (Kojima et al., 2019) were downloaded from EBI ENA (accessions PRJNA321732, PRJNA476515), trimmed and mapped to mm10 as described above. The paired end *Mybl1* data was mapped using mate inner distance and mate standard deviations of 30 and 68 respectively. Accepted hits from Tophat were filtered as described above and uniquely mapping reads falling within GencodeBasic VM18 genes counted using htseq-count v0.11.2 (Anders et al., 2015) in intersection-nonempty mode. The ENSMUST00000174651.1 transcript in the GencodeBasic VM18 annotation, which appears to be a *Moap1* transcript originating from an alternative upstream promoter, was manually re-assigned from the RP24-234J3.3 gene to *Moap1* to circumvent ambiguity in htseq-count assigning reads to *Moap1*. EdgeR was used to normalize the counts per million mapped fragments in each sample using trimmed means, data for genes of interest (*Moap1*, *Pnma1*) selected from the dataset, and Student's t-test used

to assess statistical significance between *Mybl1*$^{+/-}$ and *Mybl1*$^{-/-}$ P14 testis samples, or between *Stra8*$^{+/-}$ highSTRA8 preleptotene spermatocyte and *Stra8*$^{-/-}$ preleptotene spermatocyte samples.

FPKMs from RNA-seq for opossum from purified spermatocyte/spermatid and multitissue (Lesch et al., 2016; Marin et al., 2017) were downloaded from NCBI GEO with the following accessions: GSE68507, GSE97367.

Analysis of mammalian ChIPseq data (mouse)

Mybl1 and Stra8 ChIPseq data from mouse testes (Kojima et al., 2019; Zhou et al., 2017) were downloaded from EBI ENA (accessions PRJNA321732, PRJNA476515), trimmed as described for RNAseq data, then aligned to the mm10 assembly of the mouse genome using Bowtie v2.2.6 (Langmead and Salzberg, 2012). Bowtie output was filtered to remove PCR duplicates marked by PicardTools v2.17.11 (http://broadinstitute.github.io/picard/), and to remove reads mapping to mitochondrial or blacklisted regions of the genome (https://www.encodeproject.org/files/ENCFF023CZC/), unmapped reads, non-primary alignments and reads with a quality score below 5. Bedtools (Quinlan and Hall, 2010) was used to convert the Bowtie alignments to ENCODE tagAlign format, and MACS v2.1.1 (Zhang et al., 2008) used to call peaks on pooled ChIP samples relative to pooled input controls using default settings ($q < 0.05$) and to generate Bedgraphs showing fold enrichment in pooled ChIP relative to input samples. For Stra8 ChIPseq, the fold-enrichment for anti-FLAG ChIP in control wild-type samples was then subtracted from the fold-enrichment for the anti-FLAG ChIP in experimental *Stra8*$^{FLAG/FLAG}$ samples. For Mybl1 ChIPseq, anti-Mybl1 ChIPseq from *Mybl1*$^{+/-}$ testes was compared to *Mybl1*$^{+/-}$ input controls. ChIPseq bedgraphs and peak co-ordinates were visualised using Gviz (Hahne and Ivanek, 2016). Distances from Repeatmasker-annotated MamGyp-int loci and GencodeBasic VM18 genes overlapping those loci to the nearest Stra8 and Mybl1 ChIPseq peaks were determined using BEDtools v2.26.0 (Quinlan and Hall, 2010).

Analysis of Dazl CLIP and DAZL RIP mammalian data (mouse, human)

Dazl CLIP tag locations from mouse testes (Zagore et al., 2018) were downloaded from GEO (accession GSE108181) and the genomic co-ordinates lifted over from mm9 to mm10 using the UCSC liftOver tool (Haeussler et al., 2019). DAZL RIP data from human ovaries (Rosario et al., 2017) (available in EBI ENA, PRJNA321858) was trimmed and aligned to the hg38 assembly of the human genome as described for the RNAseq data using a mate inner distance of 260 and mate standard

deviation of 110. Tophat output was filtered, then reads in genes or repeats counted using htseq-count or BEDTools and normalized in EdgeR using the total number of mapped fragments as the library size as described for the RNAseq data. To assess *MOAP1* and *PNMA1* behaviour in the htseq-count data, EdgeR, low abundance genes were removed using *filterByExpr(count=15, min.count=10), glmLRT* used to determine differentially abundant genes in a paired experimental design, *MOAP1* and *PNMA1* data extracted from the resulting DGELRT object. and false discovery rate used to correct p-values for multiple-testing. To determine enriched retrotransposon sequences in the anti-DAZL samples, repName-aggregated repeat count data for retrotransposons (LINE, SINE and LTR repeat classes) were selected then low abundance retrotransposons removed using *filterByExpr(count=15, min.count=10)*. *glmLRT* was used to determine differentially abundant retrotransposons in a paired experimental design, and false discovery rate used to correct p-values for multiple-testing. Data for retrotransposons belonging to the *Gypsy* repeat family were plotted.

REFERENCES

Anders, S., Pyl, P.T., and Huber, W. (2015). HTSeq—a Python framework to work with high-throughput sequencing data. Bioinformatics *31*, 166–169.

Anderson, E.L., Baltus, A.E., Roepers-Gajadien, H.L., Hassold, T.J., de Rooij, D.G., van Pelt, A.M.M., and Page, D.C. (2008). Stra8 and its inducer, retinoic acid, regulate meiotic initiation in both spermatogenesis and oogenesis in mice. Proc. Natl. Acad. Sci. *105*, 14976–14980.

Arkhipova, I., and Meselson, M. (2005). Deleterious transposable elements and the extinction of asexuals. Bioessays *27*, 76–85.

Aye, M., Irwin, B., Beliakova-Bethell, N., Chen, E., Garrus, J., and Sandmeyer, S. (2004). Host factors that affect Ty3 retrotransposition in Saccharomyces cerevisiae. Genetics *168*, 1159–1176.

Bao, J., and Yan, W. (2012). Male germline control of transposable elements. Biol. Reprod. *86*, 161–162.

Barau, J., Teissandier, A., Zamudio, N., Roy, S., Nalesso, V., Hérault, Y., Guillou, F., and Bourc'his, D. (2016). The DNA methyltransferase DNMT3C protects male germ cells from transposon activity. Science (80-.). *354*, 909–912.

Beliakova-Bethell, N., Beckham, C., Giddings, T.H., Winey, M., Parker, R., and Sandmeyer, S. (2006). Virus-like particles of the Ty3 retrotransposon assemble in association with P-body components. Rna *12*, 94–101.

Benjamin, K.R., Zhang, C., Shokat, K.M., and Herskowitz, I. (2003). Control of landmark events in meiosis by the CDK Cdc28 and the meiosis-specific kinase Ime2. Genes Dev. *17*, 1524–1539.

Berchowitz, L.E., Gajadhar, A.S., Werven, F.J. Van, Rosa, A. a De, Weissman, J.S., White, F.M., Amon, A., van Werven, F.J., De Rosa, A. a, Samoylova, M.L., et al. (2013). A developmentally regulated translational control pathway establishes the meiotic chromosome segregation pattern. Genes Dev. *27*, 2147–2163.

Berchowitz, L.E., Kabachinski, G., Walker, M.R., Carlile, T.M., Gilbert, W.V., Schwartz, T.U., and Amon, A. (2015). Regulated Formation of an Amyloid-like Translational Repressor Governs Gametogenesis. Cell *163*, 406–418.

Bilanchone, V.W., Claypool, J.A., Kinsey, P.T., and Sandmeyer, S.B. (1993). Positive and negative regulatory elements control expression of the yeast retrotransposon Ty3. Genetics *134*, 685–700.

Bolcun-Filas, E., Bannister, L.A., Barash, A., Schimenti, K.J., Hartford, S.A., Eppig, J.J., Handel, M.A., Shen, L., and Schimenti, J.C. (2011). A-MYB (MYBL1) transcription factor is a master regulator of male meiosis. Development *138*, 3319–3330.

Bourc'his, D., and Bestor, T.H. (2004). Meiotic catastrophe and retrotransposon reactivation in male germ cells lacking Dnmt3L. Nature *431*, 96–99.

Bourque, G., Burns, K.H., Gehring, M., Gorbunova, V., Seluanov, A., Hammell, M., Imbeault, M., Izsvák, Z., Levin, H.L., and Macfarlan, T.S. (2018). Ten things you should know about transposable elements. Genome Biol. *19*, 1–12.

Brar, G. a., Yassour, M., Friedman, N., Regev, A., Ingolia, N.T., and Weissman, J.S. (2012). High-resolution view of the yeast meiotic program revealed by ribosome profiling. Science (80-.). *335*, 552–557.

Brion, C., Legrand, S., Peter, J., Caradec, C., Pflieger, D., Hou, J., Friedrich, A., Llorente, B., and Schacherer, J. (2017). Variation of the meiotic recombination landscape and properties over a broad

evolutionary distance in yeasts. PLoS Genet. *13*, 1–21.

Campillos, M., Doerks, T., Shah, P.K., and Bork, P. (2006). Computational characterization of multiple Gag-like human proteins. Trends Genet. *22*, 585–589.

Carlile, T.M., and Amon, A. (2008). Meiosis I is established through division-specific translational control of a cyclin. Cell *133*, 280–291.

Carpenter, K., Bell, R.B., Yunus, J., Amon, A., and Berchowitz, L.E. (2018). Phosphorylation-mediated clearance of amyloid-like assemblies in meiosis. Dev. Cell *45*, 392–405.

Chu, S., Derisi, J., Eisen, M., Mulholland, J., Botstein, D., Brown, P.O., and Herskowitz, I. (1998). The Transcriptional Program of Sporulation in Budding Yeast. Science (80-.). *282*, 699–705.

Chuong, E.B., Elde, N.C., and Feschotte, C. (2017). Regulatory activities of transposable elements: from conflicts to benefits. Nat. Rev. Genet. *18*, 71.

Cosby, R.L., Chang, N.-C., and Feschotte, C. (2019). Host–transposon interactions: conflict, cooperation, and cooption. Genes Dev. *33*, 1098–1116.

Crichton, J.H., Dunican, D.S., MacLennan, M., Meehan, R.R., and Adams, I.R. (2014). Defending the genome from the enemy within: mechanisms of retrotransposon suppression in the mouse germline. Cell. Mol. Life Sci. *71*, 1581–1605.

Cristofari, G., Gabus, C., Ficheux, D., Bona, M., Le Grice, S.F.J., and Darlix, J.-L. (1999). Characterization of active reverse transcriptase and nucleoprotein complexes of the yeast retrotransposon Ty3 in vitro. J. Biol. Chem. *274*, 36643–36648.

Dechaud, C., Volff, J.-N., Schartl, M., and Naville, M. (2019). Sex and the TEs: transposable elements in sexual development and function in animals. Mob. DNA *10*, 42.

Descrimes, M., Zouari, Y. Ben, Wery, M., Legendre, R., Gautheret, D., and Morillon, A. (2015). VING: a software for visualization of deep sequencing signals. BMC Res. Notes *8*, 419.

Dobin, A., Davis, C.A., Schlesinger, F., Drenkow, J., Zaleski, C., Jha, S., Batut, P., Chaisson, M., and Gingeras, T.R. (2013). STAR: ultrafast universal RNA-seq aligner. Bioinformatics *29*, 15–21.

Farabaugh, P.J., Zhao, H., and Vimaladithan, A. (1993). A novel programed frameshift expresses the POL3 gene of retrotransposon Ty3 of yeast: Frameshifting without tRNA slippage. Cell *74*, 93–103.

Feng, Y.-X., Moore, S.P., Garfinkel, D.J., and Rein, A. (2000). The genomic RNA in Ty1 virus-like particles is dimeric. J. Virol. *74*, 10819–10821.

Frankish, A., Diekhans, M., Ferreira, A.-M., Johnson, R., Jungreis, I., Loveland, J., Mudge, J.M., Sisu, C., Wright, J., and Armstrong, J. (2019). GENCODE reference annotation for the human and mouse genomes. Nucleic Acids Res. *47*, D766–D773.

Garfinkel, D.J., Boeke, J.D., and Fink, G.R. (1985). Ty element transposition: reverse transcriptase and virus-like particles. Cell *42*, 507–517.

Gnügge, R.J. (2015). Engineering of synthetic gene regulatory networks in Saccharomyces cerevisiae.

Griffith, J.L., Coleman, L.E., Raymond, A.S., Goodson, S.G., Pittard, W.S., Tsui, C., and Devine, S.E. (2003). Functional genomics reveals relationships between the retrovirus-like Ty1 element and its host Saccharomyces cerevisiae. Genetics *164*, 867–879.

Haeussler, M., Zweig, A.S., Tyner, C., Speir, M.L., Rosenbloom, K.R., Raney, B.J., Lee, C.M., Lee, B.T., Hinrichs, A.S., and Gonzalez, J.N. (2019). The UCSC genome browser database: 2019 update. Nucleic Acids Res. *47*, D853–D858.

Hahne, F., and Ivanek, R. (2016). Visualizing genomic data using Gviz and bioconductor. In Statistical

Genomics, (Springer), pp. 335–351.

Haig, D. (2016). Transposable elements: Self-seekers of the germline, team-players of the soma. Bioessays *38*, 1158–1166.

Hayward, A. (2017). Origin of the retroviruses: when, where, and how? Curr. Opin. Virol. *25*, 23–27.

Irwin, B., Aye, M., Baldi, P., Beliakova-Bethell, N., Cheng, H., Dou, Y., Liou, W., and Sandmeyer, S. (2005). Retroviruses and yeast retrotransposons use overlapping sets of host genes. Genome Res. *15*, 641–654.

Isono, E., Saito, N., Kamata, N., Saeki, Y., and Toh-e, A. (2005). Functional analysis of Rpn6p, a lid component of the 26 S proteasome, using temperature-sensitive rpn6 mutants of the yeast Saccharomyces cerevisiae. J. Biol. Chem. *280*, 6537–6547.

Jin, L., Zhang, K., Sternglanz, R., and Neiman, A.M. (2017). Predicted RNA Binding Proteins Pes4 and Mip6 Regulate mRNA Levels, Translation, and Localization during Sporulation in Budding Yeast. Mol. Cell. Biol. *37*, 10–12.

Kane, S.M., and Roth, R. (1974). Carbohydrate metabolism during ascospore development in yeast. J. Bacteriol. *118*, 8–14.

Kano, H., Godoy, I., Courtney, C., Vetter, M.R., Gerton, G.L., Ostertag, E.M., and Kazazian, H.H. (2009). L1 retrotransposition occurs mainly in embryogenesis and creates somatic mosaicism. Genes Dev. *23*, 1303–1312.

Kim, D., Pertea, G., Trapnell, C., Pimentel, H., Kelley, R., and Salzberg, S.L. (2013). TopHat2: accurate alignment of transcriptomes in the presence of insertions, deletions and gene fusions. Genome Biol. *14*, R36.

King, O.D., Gitler, A.D., and Shorter, J. (2012). The tip of the iceberg: RNA-binding proteins with prion-like domains in neurodegenerative disease. Brain Res. *1462*, 61–80.

Klutstein, M., Siegfried, Z., Gispan, A., Farkash-Amar, S., Zinman, G., Bar-Joseph, Z., Simchen, G., and Simon, I. (2010). Combination of genomic approaches with functional genetic experiments reveals two modes of repression of yeast middle-phase meiosis genes. BMC Genomics *11*, 478.

Kojima, K.K. (2018). Human transposable elements in Repbase: genomic footprints from fish to humans. Mob. DNA *9*, 2.

Kojima, M.L., de Rooij, D.G., and Page, D.C. (2019). Amplification of a broad transcriptional program by a common factor triggers the meiotic cell cycle in mice. Elife *8*, e43738.

Kokošar, J., and Kordiš, D. (2013). Genesis and regulatory wiring of retroelement-derived domesticated genes: a phylogenomic perspective. Mol. Biol. Evol. *30*, 1015–1031.

Kronja, I., and Orr-Weaver, T.L. (2011). Translational regulation of the cell cycle: when, where, how and why? Philos. Trans. R. Soc. B Biol. Sci. *366*, 3638–3652.

Langmead, B., and Salzberg, S.L. (2012). Fast gapped-read alignment with Bowtie 2. Nat. Methods *9*, 357.

Larsen, L.S.Z., Beliakova-Bethell, N., Bilanchone, V., Zhang, M., Lamsa, A., DaSilva, R., Hatfield, G.W., Nagashima, K., and Sandmeyer, S. (2008). Ty3 Nucleocapsid Controls Localization of Particle Assembly. J. Virol. *82*, 2501–2514.

Lee, B., and Amon, A. (2001). Meiosis: How to create a specialized cell cycle. Curr. Opin. Cell Biol. *13*, 770–777.

Lesch, B.J., Silber, S.J., McCarrey, J.R., and Page, D.C. (2016). Parallel evolution of male germline

epigenetic poising and somatic development in animals. Nat. Genet. *48*, 888–894.

Li, H., and Durbin, R. (2009). Fast and accurate short read alignment with Burrows-Wheeler transform. Bioinformatics *25*, 1754–1760.

Li, H., Handsaker, B., Wysoker, A., Fennell, T., Ruan, J., Homer, N., Marth, G., Abecasis, G., and Durbin, R. (2009). The sequence alignment/map format and SAMtools. Bioinformatics *25*, 2078–2079.

Longtine, M.S., Mckenzie III, A., Demarini, D.J., Shah, N.G., Wach, A., Brachat, A., Philippsen, P., and Pringle, J.R. (1998). Additional modules for versatile and economical PCR-based gene deletion and modification in Saccharomyces cerevisiae. Yeast *14*, 953–961.

MacLennan, M., García-Cañadas, M., Reichmann, J., Khazina, E., Wagner, G., Playfoot, C.J., Salvador-Palomeque, C., Mann, A.R., Peressini, P., and Sanchez, L. (2017). Mobilization of LINE-1 retrotransposons is restricted by Tex19. 1 in mouse embryonic stem cells. Elife *6*, e26152.

Malki, S., van der Heijden, G.W., O'Donnell, K.A., Martin, S.L., and Bortvin, A. (2014). A role for retrotransposon LINE-1 in fetal oocyte attrition in mice. Dev. Cell *29*, 521–533.

Marin, R., Cortez, D., Lamanna, F., Pradeepa, M.M., Leushkin, E., Julien, P., Liechti, A., Halbert, J., Brüning, T., and Mössinger, K. (2017). Convergent origination of a Drosophila-like dosage compensation mechanism in a reptile lineage. Genome Res. *27*, 1974–1987.

Martin, M. (2011). Cutadapt removes adapter sequences from high-throughput sequencing reads. EMBnet. J. *17*, 10–12.

Maxwell, P.H., and Curcio, M.J. (2007). Host factors that control long terminal repeat retrotransposons in Saccharomyces cerevisiae: implications for regulation of mammalian retroviruses. Eukaryot. Cell *6*, 1069–1080.

Merhej, J., Frigo, A., Le Crom, S., Camadro, J., Devaux, F., and Lelandais, G. (2014). bPeaks: a bioinformatics tool to detect transcription factor binding sites from ChIPseq data in yeasts and other organisms with small genomes. Yeast *31*, 375–391.

Mita, P., and Boeke, J.D. (2016). How retrotransposons shape genome regulation. Curr. Opin. Genet. Dev. *37*, 90–100.

Morawska, M., and Ulrich, H.D. (2013). An expanded tool kit for the auxin-inducible degron system in budding yeast. Yeast *30*, 341–351.

De Muyt, A., Pyatnitskaya, A., Andréani, J., Ranjha, L., Ramus, C., Laureau, R., Fernandez-Vega, A., Holoch, D., Girard, E., and Govin, J. (2018). A meiotic XPF–ERCC1-like complex recognizes joint molecule recombination intermediates to promote crossover formation. Genes Dev. *32*, 283–296.

Nocedal, I., Mancera, E., and Johnson, A.D. (2017). Gene regulatory network plasticity predates a switch in function of a conserved transcription regulator. Elife *6*, 1–20.

Nymark-McMahon, M.H., Beliakova-Bethell, N.S., Darlix, J.L., Le Grice, S.F., and Sandmeyer, S.B. (2002). Ty3 integrase is required for initiation of reverse transcription. J Virol *76*, 0–2804.

Orecchini, E., Frassinelli, L., Galardi, S., Ciafrè, S.A., and Michienzi, A. (2018). Post-transcriptional regulation of LINE-1 retrotransposition by AID/APOBEC and ADAR deaminases. Chromosom. Res. *26*, 45–59.

Peter, J., De Chiara, M., Friedrich, A., Yue, J.-X., Pflieger, D., Bergström, A., Sigwalt, A., Barre, B., Freel, K., and Llored, A. (2018). Genome evolution across 1,011 Saccharomyces cerevisiae isolates. Nature *556*, 339–344.

Pierce, M., Benjamin, K.R., Montano, S.P., Georgiadis, M.M., Winter, E., and Vershon, A.K. (2003). Sum1 and Ndt80 Proteins Compete for Binding to Middle Sporulation Element Sequences That Control

Meiotic Gene Expression. Mol. Cell. Biol. *23*, 4814–4825.

Qi, X., Daily, K., Nguyen, K., Wang, H., Mayhew, D., Rigor, P., Forouzan, S., Johnston, M., Mitra, R.D., Baldi, P., et al. (2012). Retrotransposon profiling of RNA polymerase III initiation sites. Genome Res. *22*, 681–692.

Quinlan, A.R., and Hall, I.M. (2010). BEDTools: A flexible suite of utilities for comparing genomic features. Bioinformatics *26*, 841–842.

Ramírez, F., Ryan, D.P., Grüning, B., Bhardwaj, V., Kilpert, F., Richter, A.S., Heyne, S., Dündar, F., and Manke, T. (2016). deepTools2: a next generation web server for deep-sequencing data analysis. Nucleic Acids Res. *44*, W160–W165.

Rebollo, R., Romanish, M.T., and Mager, D.L. (2012). Transposable elements: an abundant and natural source of regulatory sequences for host genes. Annu. Rev. Genet. *46*, 21–42.

Ribeiro-dos-Santos, G., Schenberg, A.C.G., Gardner, D.C.J., and Oliver, S.G. (1997). Enhancement of Ty transposition at the ADH4 and ADH2 loci in meiotic yeast cells. Mol. Gen. Genet. *254*, 555–561.

Robinson, M.D., McCarthy, D.J., and Smyth, G.K. (2010). edgeR: a Bioconductor package for differential expression analysis of digital gene expression data. Bioinformatics *26*, 139–140.

Rosario, R., Smith, R.W.P., Adams, I.R., and Anderson, R.A. (2017). RNA immunoprecipitation identifies novel targets of DAZL in human foetal ovary. MHR Basic Sci. Reprod. Med. *23*, 177–186.

Rowley, P.A., Patterson, K., Sandmeyer, S.B., and Sawyer, S.L. (2018). Control of yeast retrotransposons mediated through nucleoporin evolution. PLoS Genet. *14*, 1–24.

Sawyer, E.M., Joshi, P.R., Jorgensen, V., Yunus, J., Berchowitz, L.E., and Ünal, E. (2019). Developmental regulation of an organelle tether coordinates mitochondrial remodeling in meiosis. J. Cell Biol. *218*, 559–579.

Schindelin, J., Arganda-Carreras, I., Frise, E., Kaynig, V., Longair, M., Pietzsch, T., Preibisch, S., Rueden, C., Saalfeld, S., and Schmid, B. (2012). Fiji: an open-source platform for biological-image analysis. Nat. Methods *9*, 676–682.

Scholes, D.T., Banerjee, M., Bowen, B., and Curcio, M.J. (2001). Multiple regulators of Ty1 transposition in Saccharomyces cerevisiae have conserved roles in genome maintenance. Genetics *159*, 1449–1465.

Servant, G., Pennetier, C., and Lesage, P. (2008). Remodeling yeast gene transcription by activating the Ty1 long terminal repeat retrotransposon under severe adenine deficiency. Mol. Cell. Biol. *28*, 5543–5554.

Shen, X.-X., Opulente, D.A., Kominek, J., Zhou, X., Steenwyk, J.L., Buh, K. V, Haase, M.A.B., Wisecaver, J.H., Wang, M., and Doering, D.T. (2018). Tempo and mode of genome evolution in the budding yeast subphylum. Cell *175*, 1533–1545.

Soumillon, M., Necsulea, A., Weier, M., Brawand, D., Zhang, X., Gu, H., Barthes, P., Kokkinaki, M., Nef, S., and Gnirke, A. (2013). Cellular source and mechanisms of high transcriptome complexity in the mammalian testis. Cell Rep. *3*, 2179–2190.

Storici, F., Lewis, L.K., and Resnick, M.A. (2001). In vivo site-directed mutagenesis using oligonucleotides. Nat. Biotechnol. *19*, 773–776.

Thorvaldsdóttir, H., Robinson, J.T., and Mesirov, J.P. (2013). Integrative Genomics Viewer (IGV): high-performance genomics data visualization and exploration. Brief. Bioinform. *14*, 178–192.

Torres, E.M., Sokolsky, T., Tucker, C.M., Chan, L.Y., Boselli, M., Dunham, M.J., and Amon, A. (2007). Effects of aneuploidy on cellular physiology and cell division in haploid yeast. Science (80-.). *317*, 916–

924.

Tsuchiya, D., Yang, Y., and Lacefield, S. (2014). Positive Feedback of NDT80 Expression Ensures Irreversible Meiotic Commitment in Budding Yeast. PLoS Genet. *10*, e1004398.

Volff, J. (2006). Turning junk into gold: domestication of transposable elements and the creation of new genes in eukaryotes. Bioessays *28*, 913–922.

Volff, J. (2009). Cellular genes derived from Gypsy/Ty3 retrotransposons in mammalian genomes. Ann. N. Y. Acad. Sci. *1178*, 233–243.

Wang, L., Dou, K., Moon, S., Tan, F.J., and Zhang, Z.Z.Z. (2018). Hijacking oogenesis enables massive propagation of LINE and retroviral transposons. Cell *174*, 1082–1094.

Warren, I.A., Naville, M., Chalopin, D., Levin, P., Berger, C.S., Galiana, D., and Volff, J.-N. (2015). Evolutionary impact of transposable elements on genomic diversity and lineage-specific innovation in vertebrates. Chromosom. Res. *23*, 505–531.

Wicker, T., Sabot, F., Hua-Van, A., Bennetzen, J.L., Capy, P., Chalhoub, B., Flavell, A., Leroy, P., Morgante, M., and Panaud, O. (2007). A unified classification system for eukaryotic transposable elements. Nat. Rev. Genet. *8*, 973–982.

Winter, E. (2012). The Sum1/Ndt80 Transcriptional Switch and Commitment to Meiosis in Saccharomyces cerevisiae. Microbiol. Mol. Biol. Rev. *76*, 1–15.

Xu, L., Ajimura, M., Padmore, R., Klein, C., and Kleckner, N. (1995). NDT80, a meiosis-specific gene required for exit from pachytene in Saccharomyces cerevisiae. Mol. Cell. Biol. *15*, 6572–6581.

Yang, F., and Wang, P.J. (2016). Multiple LINEs of retrotransposon silencing mechanisms in the mammalian germline. In Seminars in Cell & Developmental Biology, (Elsevier), pp. 118–125.

Yue, J.-X.X., Li, J., Aigrain, L., Hallin, J., Persson, K., Oliver, K., Bergström, A., Coupland, P., Warringer, J., Lagomarsino, M.C., et al. (2017). Contrasting evolutionary genome dynamics between domesticated and wild yeasts. Nat. Genet. *49*, 913–924.

Zagore, L.L., Sweet, T.J., Hannigan, M.M., Weyn-Vanhentenryck, S.M., Jobava, R., Hatzoglou, M., Zhang, C., and Licatalosi, D.D. (2018). DAZL regulates germ cell survival through a network of PolyA-Proximal mRNA interactions. Cell Rep. *25*, 1225–1240.

Zhang, Y., Liu, T., Meyer, C.A., Eeckhoute, J., Johnson, D.S., Bernstein, B.E., Nusbaum, C., Myers, R.M., Brown, M., and Li, W. (2008). Model-based analysis of ChIP-Seq (MACS). Genome Biol. *9*, R137.

Zhou, L., Canagarajah, B., Zhao, Y., Baibakov, B., Tokuhiro, K., Maric, D., and Dean, J. (2017). BTBD18 regulates a subset of piRNA-generating loci through transcription elongation in mice. Dev. Cell *40*, 453–466.

KEY RESOURCES TABLE

REAGENT or RESOURCE	SOURCE	IDENTIFIER
Antibodies		
α-HA.11 Clone:16B12 (mouse)	BioLegend	Cat# 901514
α-Pgk1 (Phosphoglycerate Kinase monoclonal) (mouse)	Novex (Life Technologies)	Part# 459250
α-v5 monoclonal (mouse)	Invitrogen	Cat# 46-0705
α-FLAG (rabbit)	Sigma-Aldrich	Cat# F7425
α-VLP (Ty3) crude serum (rabbit)	Sandmeyer lab (UC Irvine)	α-VLP (Ty3) crude serum
α-VLP (Ty3) affinity purified antibody, using *E. coli* produced Gag3 protein	This study	α-VLP (Ty3) affinity purified antibody
α-mouse HRP-conjugated secondary	GE Healthcare	Cat# NA931-1ML
α-rabbit HRP-conjugated secondary	GE Healthcare	Cat# NA934V
α-V5-coupled agarose	Sigma-Aldrich	Cat# A7345-1ml
Rat α-tubulin alpha	Bio-Rad	Cat# MCA77G
α-rat-FITC	Invitrogen	Cat# 31629
Chemicals, Peptides, and Recombinant Proteins		
Halt Protease Inhibitor	ThermoFisher	Cat# 1861279
ProlongGold anti-fade reagent w/ DAPI	Invitrogen	Cat# P36935
β-Estradiol	Sigma-Aldrich	Cat# E8875
MG-132	Cayman Chemical	Cat# 10012628
Auxin (indole-3-acetic acid)	Sigma-Aldrich	Cat# 12886-25G
α-factor mating pheromone	Genscript	Cat# RP01002
Acid-washed glass beads, 425-600µm	Sigma-Aldrich	Cat# G8772-500G
0.5mm dia Zirconia/silica beads	BioSpec Products	Cat# 11079105Z
Chelex resin	Bio-Rad	Cat# 1422832
Hybond-N+ membrane	GE Healthcare	Prod# RPN203B
10% Criterion TGX Precast Midi Protein Gel, 26 well, 15 µl	Bio-Rad	Cat# 5671035
Trans-blot turbo transfer kits (Nitrocellulose)	Bio-Rad	Cat# 1704271
Illustra Probequant Columns	GE Healthcare	Prod# 28903408
Critical Commercial Assays		
AminoLink Plus Immobilization kit	Thermo Scientific	Cat# 44894
Amersham MegaPrime DNA Labeling Kit	GE Healthcare	Prod# RPN1604
Minelute kit	Qiagen	Cat# 28004
Accel-NGS 1S plus DNA library kit	Swift Biosciences	Cat# 10096
TruSeq Stranded Total Rna Kit	Illumina	Cat# RS-122-2302
Deposited data		
SK1 reference genome and other *S. cerevisiae* and *S. paradoxus* reference genomes	(Yue et al., 2017)	https://yjx1217.github.io/Yeast_PacBio_2016/data/
Raw reads for RNA-seq and ChIP-seq EBI ENA / NCBI BioProject PRJNA669383	This study	https://www.ncbi.nlm.nih.gov/bioproject/?term=PRJNA669383
Mouse reference genome: mm10 assembly	Mouse Genome Sequencing Consortium	https://genome.ucsc.edu/

REAGENT or RESOURCE	SOURCE	IDENTIFIER
RNAseq adult mouse testicular cell types, EBI ENA / NCBI BioProject accession PRJNA187158	(Soumillon et al., 2013)	https://www.ebi.ac.uk/ena/browser/view/PRJNA187158
RNAseq for P14 *Mybl1* testes EBI ENA / NCBI BIOPROJECT accession PRJNA321732	(Zhou et al., 2017)	https://www.ebi.ac.uk/ena/browser/view/PRJNA321732
RNAseq *Stra8* preleptotene spermatocytes EBI ENA / NCBI BIOPROJECT accession PRJNA476515	(Kojima et al., 2019)	https://www.ebi.ac.uk/ena/browser/view/PRJNA476515
Repeatmasker-annotated loci in mm10	Institute for Systems Biology	http://repeatmasker.org/species/mm.html
GencodeBasic VM18 annotation NCBI GEO accession GSE108181	GENCODE project	https://www.gencodegenes.org/mouse/release_M18.html
Mybl1 ChIPseq data from mouse testes EBI ENA / NCBI BIOPROJECT accession PRJNA321732	(Kojima et al., 2019)	https://www.ebi.ac.uk/ena/browser/view/PRJNA321732
Stra8 ChIPseq data from mouse testes EBI ENA / NCBI BIOPROJECT accession PRJNA476515	(Kojima et al., 2019)	https://www.ebi.ac.uk/ena/browser/view/PRJNA476515
Dazl CLIP from mouse testes NCBI GEO accession GSE108181	(Zagore et al., 2018)	https://www.ncbi.nlm.nih.gov/geo/query/acc.cgi?acc=GSE108181
RNA-seq for opossum (purified spermatocyte/spermatid) NCBI GEO accession GSE68507	(Lesch et al., 2016)	https://www.ncbi.nlm.nih.gov/geo/query/acc.cgi?acc=GSE68507
RNA-seq from opossum (multitissue) NCBI GEO accession GSE97367	(Marin et al., 2017)	https://www.ncbi.nlm.nih.gov/geo/query/acc.cgi?acc=GSE97367
Human reference genome: hg38 assembly	Genome Reference Consortium	https://genome.ucsc.edu/
Repeatmasker-annotated loci in hg38	Institute for Systems Biology	http://repeatmasker.org/species/hg.html
DAZL RIP from human ovaries EBI ENA / NCBI BIOPROJECT accession PRJNA321858	(Rosario et al., 2017)	https://www.ebi.ac.uk/ena/browser/view/PRJNA321858
Experimental Models: Organisms/Strains		
All lab strains are *S. cerevisiae,* of SK1 background (see table S1)	(Kane and Roth, 1974)	ATCC: 204722
Oligonucleotides		
FW primer for Ty3 Northern probe: 5'-GCTTTATGGATCAAATCCCC-3'	This paper	N/A
RV primer for Ty3 Northern probe: 5'-AGCATATATCGGAAGTGGTGGA-3'	This paper	N/A
FW primer for CA Northern probe: 5'-GCTTTATGGATCAAATCCCC-3'	This paper	N/A
RV primer for CA Northern probe: 5'-ACCGATGATAGTGTCTCC-3'	This paper	N/A
FW primer for PR Northern probe: 5'-TATATCGCCATCCCCGAGATGG-3'	This paper	N/A
RV primer for PR Northern probe: 5'-GACAACATTGGAGTATTTTCC-3'	This paper	N/A
FW primer for RT Northern probe: 5'-GATAACAAGTTCATTGTTCCC-3'	This paper	N/A
RV primer for RT Northern probe: 5'-GGAGCAATTTGGAATGAATCG-3'	This paper	N/A

REAGENT or RESOURCE	SOURCE	IDENTIFIER
FW primer for IN Northern probe: 5'-GACGCCTCAAAAGACGGC-3'	This paper	N/A
RV primer for IN Northern probe: 5'-TTCCAAGTGTTCTAGTAGG-3'	This paper	N/A
Recombinant DNA		
Construct: *ura3::pGPD-GAL4(848).ER::URA3*	(Benjamin et al., 2003)	N/A
Construct: *pGAL-NDT80::TRP1*	(Benjamin et al., 2003)	N/A
Construct: *CLB3-3HA:kanMX6*	(Carlile and Amon, 2008)	N/A
Construct: *RIM4-3V5::His3MX6*	(Berchowitz et al., 2013)	N/A
Construct: *RIM4-AID*-6FLAG::HYGR*	this paper	N/A
Construct: *rim4Δ138-3V5::His3MX6*	(Berchowitz et al., 2015)	N/A
Construct: *rim4Δ271-3V5::His3MX6*	(Berchowitz et al., 2015)	N/A
Construct: *pdr5::TRP1*	(Torres et al., 2007)	N/A
Construct: *rpn6-1::His3MX6*	(Carpenter et al., 2018)	N/A
Construct: *ty3Δ*	this paper	N/A
Construct: *MSE-His3MX6-Ty3*	this paper	N/A
Construct: *kanMX6-Ty3*	this paper	N/A
Construct: *kanMX6-mse(-269)Δ::AAAAAA-+TT(-163)-mse(-79)Δ::AAAAAA-Ty3*	this paper	N/A
Construct: *his3::pGPD1-OsTIR1::His3MX6*	this paper	N/A
Construct: his3::pRIM4-OsTIR1::His3MX6	this paper	N/A
Construct: *SUM1-3V5-IAA7-kanMX*	this paper	N/A
Plasmid: pHyg-AID*-6FLAG (to build *RIM4-AID*-6FLAG::HYGR*)	(Morawska and Ulrich, 2013)	https://www.addgene.org/99519/
Plasmid: pFA6a-kanMX6 (to build *kanMX6-Ty3* and *kanMX6-mse(-269)Δ::AAAAAA-TT(-163)-mse(-79)Δ::AAAAAA-Ty3)*)	(Longtine et al., 1998)	https://www.addgene.org/39296/
Plasmid: pLZL2422 (to produce Gag3 protein to purify α-VLP from crude serum)	(Larsen et al., 2008)	N/A
Plasmid: pRG206MX (to build *ty3Δ::URA3MX* (popin) prior to popout)	(Gnügge, 2015)	https://www.addgene.org/64536/
Plasmid: pFA6a-His3MX6 (to build *MSE-His3MX6-Ty3*)	(Longtine et al., 1998)	https://www.addgene.org/41596/
Plasmid: pUB976 (to make *his3::pRIM4-OsTIR1::His3MX6* and *his3::pGPD1-OsTIR1::His3MX6*)	(Sawyer et al., 2019)	N/A
Software and Algorithms		
R v3.6.1	R Core Team	https://www.R-project.org/
R studio v1.1.383	R Core Team	http://www.rstudio.com/
STAR v020201	(Dobin et al., 2013)	https://github.com/alexdobin/STAR

REAGENT or RESOURCE	SOURCE	IDENTIFIER
Ving software v beta1.1	(Descrimes et al., 2015)	http://vm-gb.curie.fr/ving/
cutadapt v2.10	(Martin, 2011)	https://cutadapt.readthedocs.io/en/stable/index.html
Bowtie2 v2.3.4 (yeast analysis) and v2.2.6 (mammals analysis)	(Langmead and Salzberg, 2012)	https://anaconda.org/bioconda/bowtie2/files
SAMtools v1.6	(Li and Durbin, 2009)	http://www.htslib.org/
Picard tool MarkDuplicates v 2.23.3 (yeast analysis) and v2.17.11 (mammals analysis)	Broad Institute	https://broadinstitute.github.io/picard/
Deeptools bamcoverage	(Ramírez et al., 2016)	https://deeptools.readthedocs.io/en/develop/content/tools/bamCoverage.html
Yeast ChIP normalization custom script	Available upon request	N/A
bpeaks v1.2	(Merhej et al., 2014)	https://cran.r-project.org/web/packages/bPeaks/index.html
IGV v2.8.9	(Thorvaldsdóttir et al., 2013)	http://software.broadinstitute.org/software/igv/
Fiji software	(Schindelin et al., 2012)	https://fiji.sc/
TrimGalore 0.4.1	The Babraham Institute	https://github.com/FelixKrueger/TrimGalore
Tophat v2.1.0	(Kim et al., 2013)	https://ccb.jhu.edu/software/tophat/index.shtml
EdgeR	(Robinson et al., 2010)	http://bioconductor.org/packages/release/bioc/html/edgeR.html
Htseq-count v0.11.2	(Anders et al., 2015)	https://htseq.readthedocs.io/en/release_0.11.1/count.html
bedtools v2.26.0	(Quinlan and Hall, 2010)	https://github.com/arq5x/bedtools2/releases/tag/v2.26.0
MACS v2.1.1	(Zhang et al., 2008)	https://github.com/macs3-project/MACS
Gviz	(Hahne and Ivanek, 2016)	http://bioconductor.org/packages/release/bioc/html/Gviz.html
UCSC liftOver tool	(Haeussler et al., 2019)	https://genome.ucsc.edu/cgi-bin/hgLiftOver
Other		
DeltaVision Elite Microcope	GE Healthcare	Prod #: 29065728
FastPrep-24	MP biomedicals	Cat# 6004500
Criterion Vertical Electrophoresis Cell	Bio-Rad	Cat# 1656001
Trans-Blot Turbo Transfer System	Bio-Rad	Cat# 1704150

Figure 1

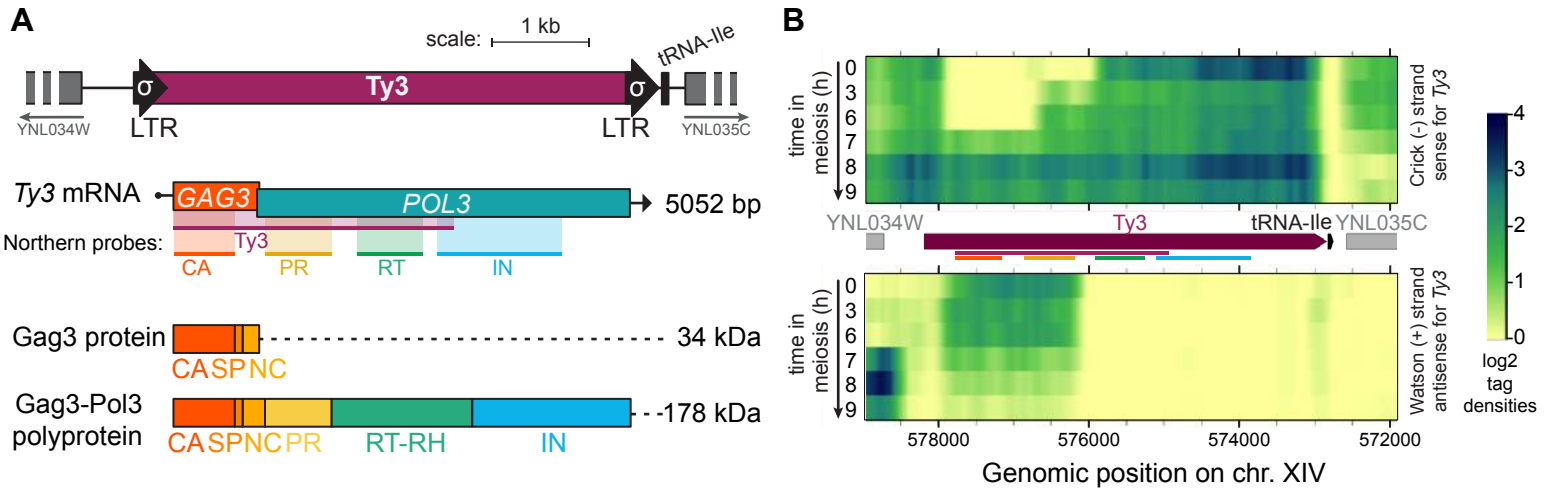

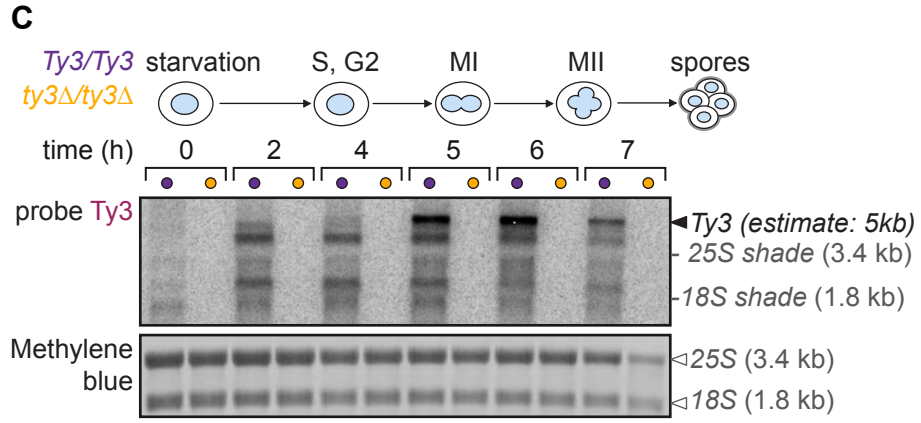

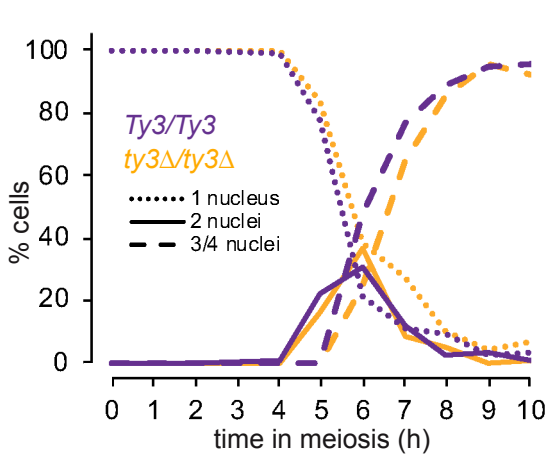

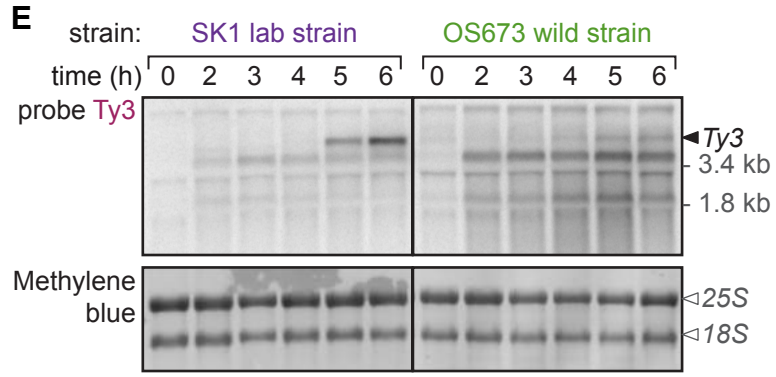

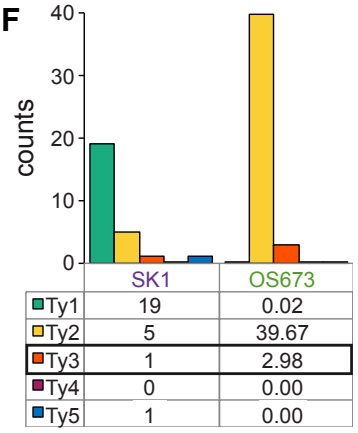

	SK1	OS673
Ty1	19	0.02
Ty2	5	39.67
Ty3	1	2.98
Ty4	0	0.00
Ty5	1	0.00

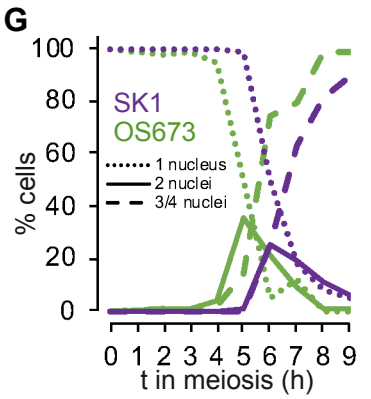

Figure 2

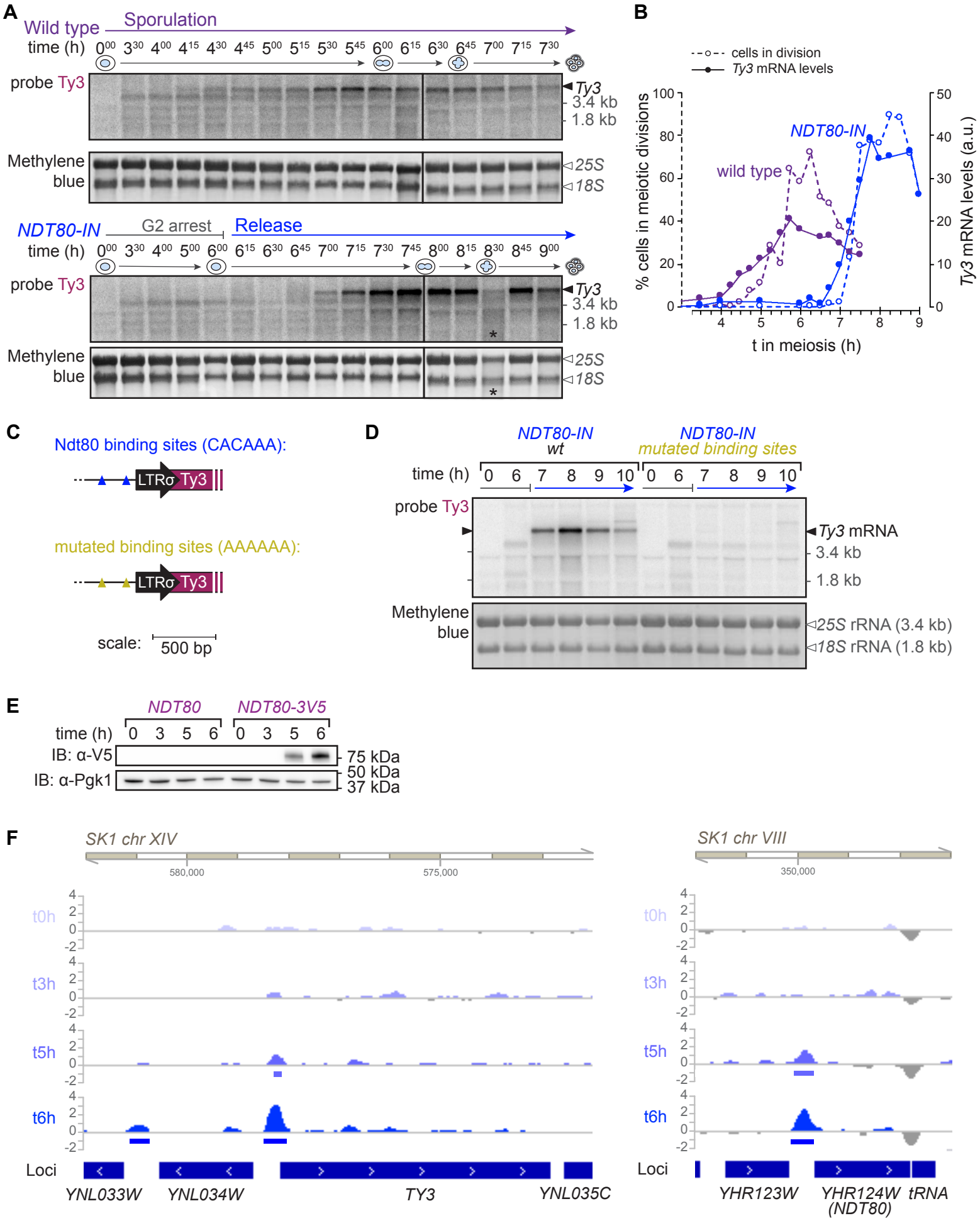
A
Wild type
Sporulation
time (h)
probe Ty3
Ty3
3.4 kb
1.8 kb
Methylene blue
25S
18S
NDT80-IN
G2 arrest
Release
B
cells in division
Ty3 mRNA levels
NDT80-IN
wild type
% cells in meiotic divisions
Ty3 mRNA levels (a.u.)
t in meiosis (h)
C
Ndt80 binding sites (CACAAA):
LTRσ Ty3
mutated binding sites (AAAAAA):
scale:
500 bp
D
NDT80-IN wt
NDT80-IN mutated binding sites
time (h)
probe Ty3
Ty3 mRNA
3.4 kb
1.8 kb
Methylene blue
25S rRNA (3.4 kb)
18S rRNA (1.8 kb)
E
NDT80
NDT80-3V5
time (h)
IB: α-V5
IB: α-Pgk1
75 kDa
50 kDa
37 kDa
F
SK1 chr XIV
580,000
575,000
SK1 chr VIII
350,000
t0h
t3h
t5h
t6h
Loci
YNL033W
YNL034W
TY3
YNL035C
YHR123W
YHR124W (NDT80)
tRNA

Figure 3

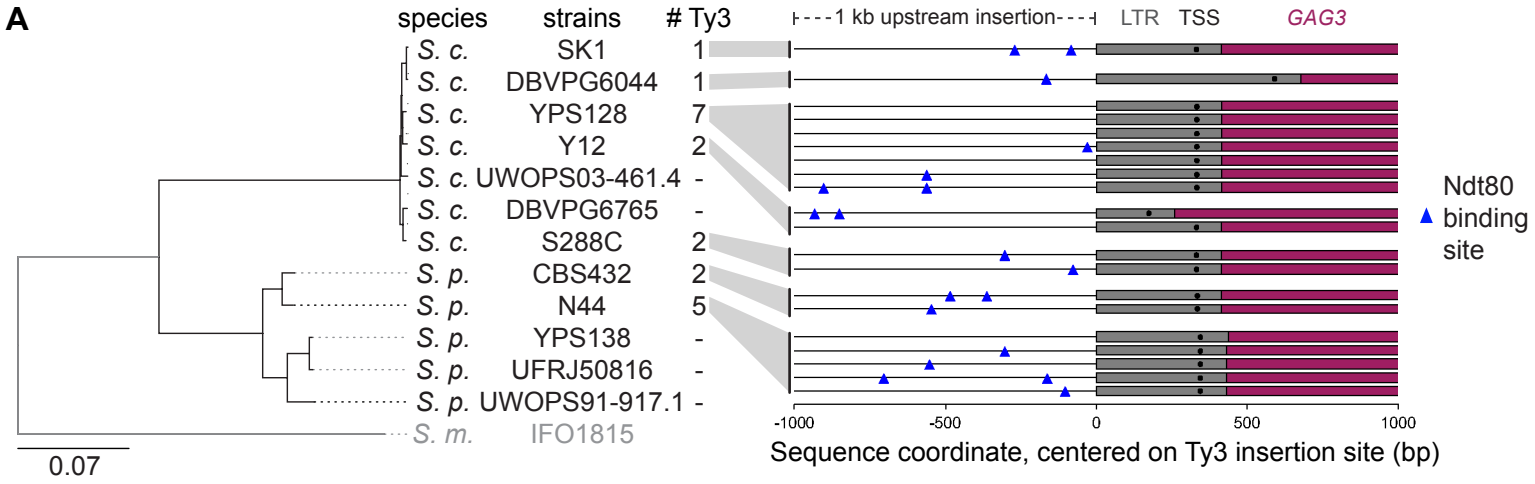
A
species
strains
Ty3
S. c. SK1 1
S. c. DBVPG6044 1
S. c. YPS128 7
S. c. Y12 2
S. c. UWOPS03-461.4 -
S. c. DBVPG6765 -
S. c. S288C 2
S. p. CBS432 2
S. p. N44 5
S. p. YPS138 -
S. p. UFRJ50816 -
S. p. UWOPS91-917.1 -
S. m. IFO1815
0.07
1 kb upstream insertion
LTR
TSS
GAG3
Ndt80 binding site
-1000
-500
0
500
1000
Sequence coordinate, centered on Ty3 insertion site (bp)

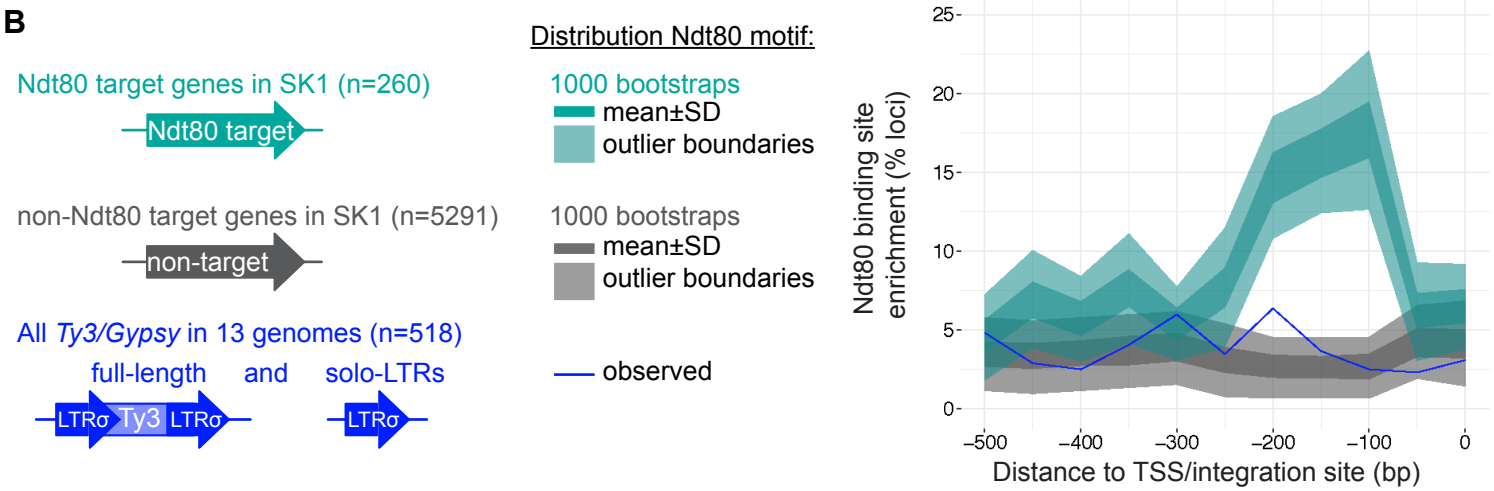
B
Ndt80 target genes in SK1 (n=260)
Ndt80 target
non-Ndt80 target genes in SK1 (n=5291)
non-target
All Ty3/Gypsy in 13 genomes (n=518)
full-length and solo-LTRs
LTRσ Ty3 LTRσ
LTRσ
Distribution Ndt80 motif:
1000 bootstraps
mean±SD
outlier boundaries
1000 bootstraps
mean±SD
outlier boundaries
observed
Ndt80 binding site enrichment (% loci)
25
20
15
10
5
0
−500
−400
−300
−200
−100
0
Distance to TSS/integration site (bp)

Figure 4

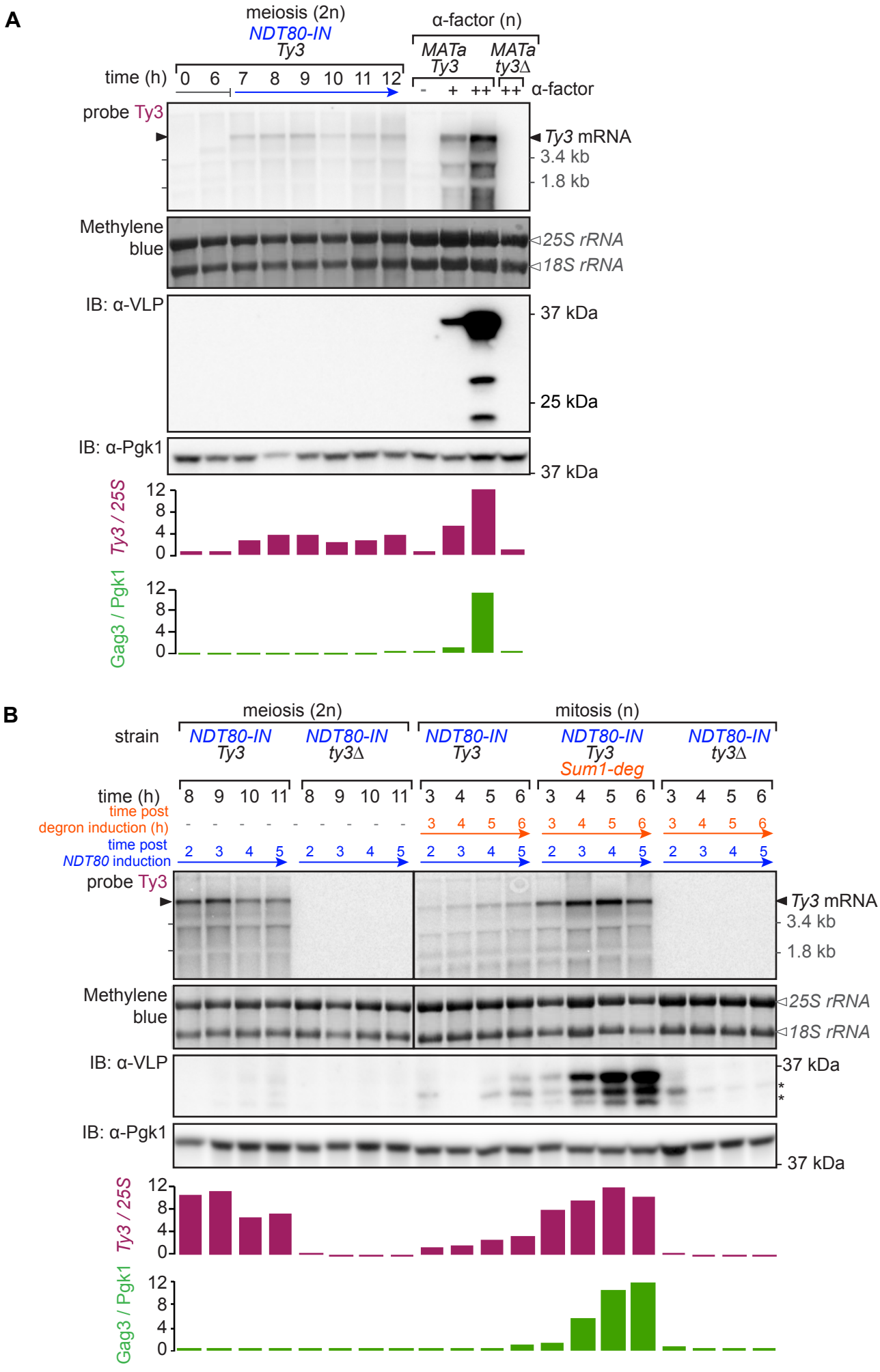
A
meiosis (2n)
NDT80-IN
Ty3
α-factor (n)
MATa
Ty3
MATa
ty3Δ
time (h)
0 6 7 8 9 10 11 12
- + ++ ++ α-factor
probe Ty3
Ty3 mRNA
3.4 kb
1.8 kb
Methylene
blue
25S rRNA
18S rRNA
IB: α-VLP
37 kDa
25 kDa
IB: α-Pgk1
37 kDa
Ty3 / 25S
Gag3 / Pgk1
12
8
4
0
B
meiosis (2n)
mitosis (n)
strain
NDT80-IN
Ty3
NDT80-IN
ty3Δ
NDT80-IN
Ty3
NDT80-IN
Ty3
Sum1-deg
NDT80-IN
ty3Δ
time (h)
8 9 10 11 8 9 10 11 3 4 5 6 3 4 5 6 3 4 5 6 3 4 5 6
time post
degron induction (h)
- - - - - - - - - 3 4 5 6 3 4 5 6 3 4 5 6
time post
NDT80 induction
2 3 4 5 2 3 4 5 2 3 4 5 2 3 4 5 2 3 4 5
probe Ty3
Ty3 mRNA
3.4 kb
1.8 kb
Methylene
blue
25S rRNA
18S rRNA
IB: α-VLP
37 kDa
IB: α-Pgk1
37 kDa
Ty3 / 25S
Gag3 / Pgk1
12
8
4
0

Figure 5

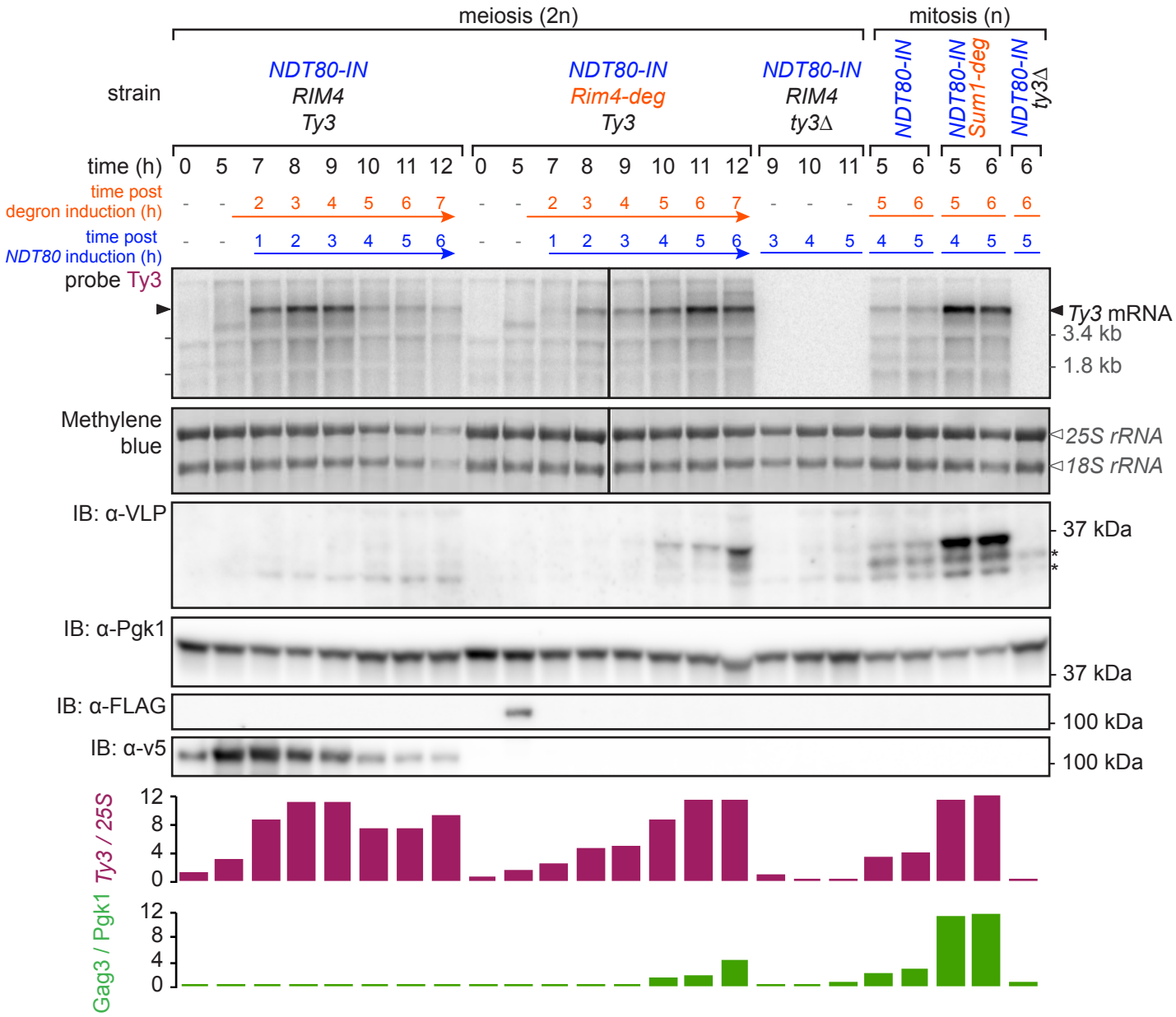
meiosis (2n)
mitosis (n)
strain
NDT80-IN RIM4 Ty3
NDT80-IN Rim4-deg Ty3
NDT80-IN RIM4 ty3Δ
NDT80-IN
NDT80-IN Sum1-deg
NDT80-IN ty3Δ
time (h)
time post degron induction (h)
time post NDT80 induction (h)
probe Ty3
Ty3 mRNA
3.4 kb
1.8 kb
Methylene blue
25S rRNA
18S rRNA
IB: α-VLP
37 kDa
IB: α-Pgk1
37 kDa
IB: α-FLAG
100 kDa
IB: α-v5
100 kDa
Ty3 / 25S
Gag3 / Pgk1

Figure 6

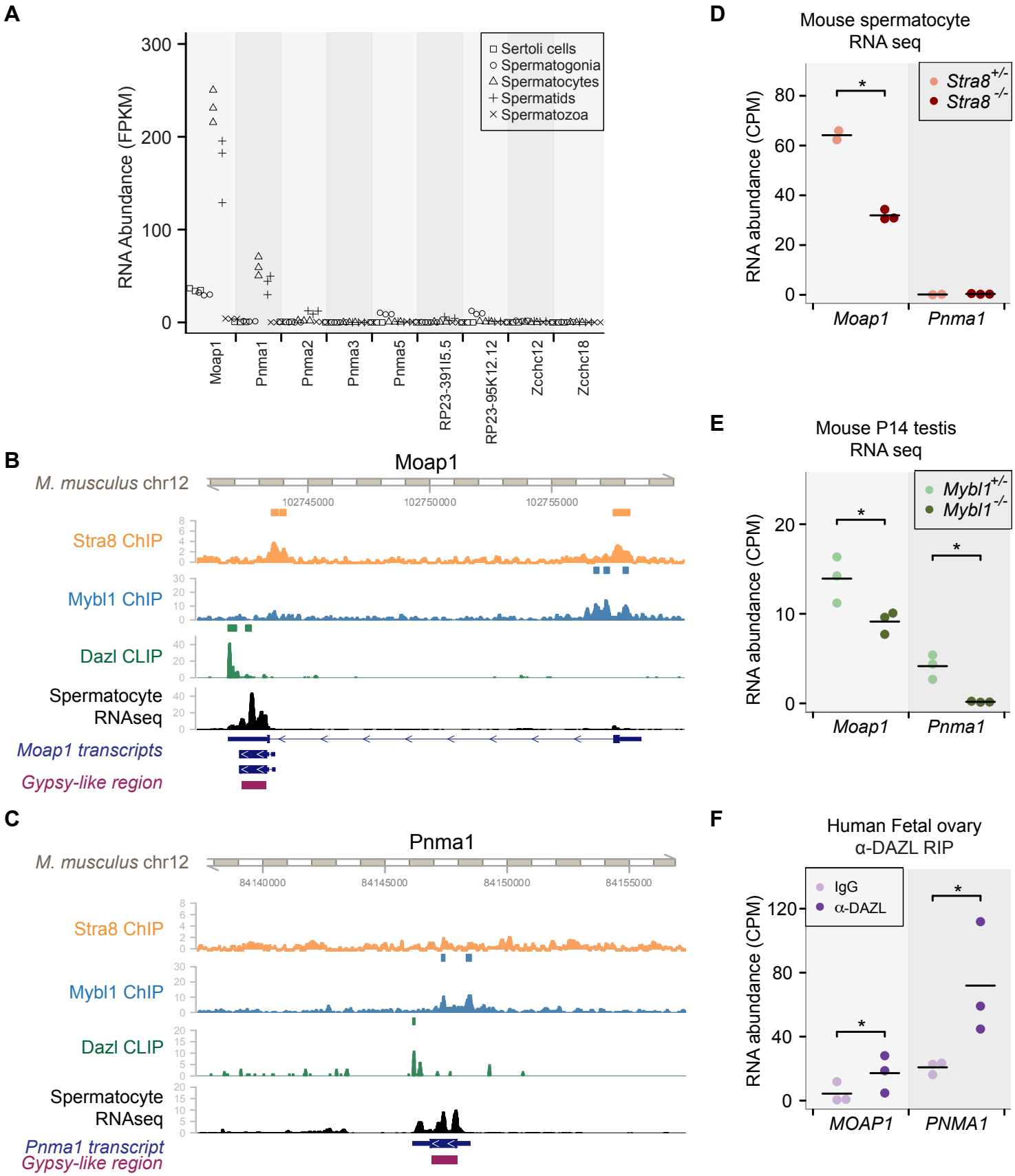
A
RNA Abundance (FPKM)
300
200
100
0
Sertoli cells
Spermatogonia
Spermatocytes
Spermatids
Spermatozoa
Moap1
Pnma1
Pnma2
Pnma3
Pnma5
RP23-391I5.5
RP23-95K12.12
Zcchc12
Zcchc18
B
Moap1
M. musculus chr12
102745000
102750000
102755000
Stra8 ChIP
Mybl1 ChIP
Dazl CLIP
Spermatocyte RNAseq
Moap1 transcripts
Gypsy-like region
C
Pnma1
M. musculus chr12
84140000
84145000
84150000
84155000
Stra8 ChIP
Mybl1 ChIP
Dazl CLIP
Spermatocyte RNAseq
Pnma1 transcript
Gypsy-like region
D
Mouse spermatocyte RNA seq
RNA abundance (CPM)
Stra8+/-
Stra8-/-
Moap1
Pnma1
E
Mouse P14 testis RNA seq
RNA abundance (CPM)
Mybl1+/-
Mybl1-/-
Moap1
Pnma1
F
Human Fetal ovary α-DAZL RIP
RNA abundance (CPM)
IgG
α-DAZL
MOAP1
PNMA1

SUPPLEMENTAL FIGURE LEGENDS

Figure S1: *Ty3* mRNA is full-length and is not required for meiotic progression, related to Figure 1

(A) Heterozygous *Ty3/ty3Δ* diploid (B838, blue) and homozygous *ty3Δ/ty3Δ* diploid (B837, yellow) do not exhibit spore viability defect compared to wild type *Ty3/Ty3* (B47, purple). Diploid strains were sporulated for the experiment shown in Figure 1C-D, and sporulation cultures were kept over week-end at 30ºC with shaking, and a sample was collected for tetrad dissection. Spore viability was assessed as the number of colony-forming spores after 2 days on YPD at 30ºC, relative to the number of dissected spores (n is indicated above bars).
(B) Homozygous *ty3Δ/ty3Δ* diploid (B837, yellow) do not exhibit growth defect compared to wild type *Ty3/Ty3* (B47, purple). Mitotic growth curves were determined from OD_{600} measurements of cells grown in YPD using a Tecan plate reader with shaking (n = 4, error bars indicate SEM).
(C) The *Ty3* locus produces full-length mRNA. RNA samples from either wild type diploid SK1 meiosis (B47, purple) or NDT80-IN diploid SK1 meiosis (B48, blue) were analyzed using the 'CA', 'PR', 'RT', and 'IN' probes (see Figure 1). In each case, the top band corresponding to the full-length mRNA is observed.

Figure S2: *Ty3* is transcriptionally activated by Ndt80, related to Figure 2

(A) *Ty3* full-length mRNA is not expressed when *NDT80* is not induced in meiosis. Meiosis was induced in two wild type strains (B371, pink and B47, purple) and *NDT80-IN* (B48) cells. *NDT80-IN* cells were either released from the G2 block by addition of 1 μM β-estradiol at 6 h (blue) or not induced (gray). Shown is Northern blot analysis of *Ty3* mRNA with annotation same as Figure 1C.
(B) Meiotic progression and *Ty3* full-length mRNA quantification in wild-type, induced, and uninduced *NDT80*. Dashed lines/left axis: Kinetics of meiotic divisions determined by α-tubulin immunofluorescence analysis (quantification of cells with one or two division spindles). Solid lines/right axis: Quantification of full-length *Ty3* mRNA.

Shown are representative results of 2 biological replicates.

Figure S3: Meiotic *Ty3* transcription is not governed by elements within the 5' LTR, related to Figure 2

(A) Diagram of endogenous and interrupted *Ty3* upstream context. Blue triangles indicate Ndt80 binding sites (-79 and -269 bp upstream *Ty3* in the endogenous context, shifted to -1,446 and -1,636 bp upon *His3MX* insertion). **(B)** Sporulation was induced in *NDT80-IN* strains containing the wild type *Ty3* configuration (B48, blue), or with an integrated *His3MX* cassette that separates *Ty3* from its upstream genetic context (B1436, orange) as in A. *Ty3* and *rRNA* RNA levels are shown.

Figure S4: Post-transcriptional repression of *Ty3* is specific to meiosis, related to Figure 4

(A) The absence of Gag3 protein in meiosis is not due to RNA degradation or proteasomal degradation. Meiosis was induced in four experimental conditions: wild type (B48), proteasome defective strain *rpn6-1* (B207), wild type + MG-132, and *pdr5*Δ (B171) + MG-132. Proteasome inhibitor MG-132 was added at 6 h to 50 µM. Meiotic cells were released from the G2 block by addition of 1 µM β-estradiol at 6 h. Mitotic induction of *NDT80* (with and without Sum1-deg) was conducted as in Figure 3B. *Ty3* mRNA (black arrow) and *rRNA* (white arrows) levels and Gag3 and Pgk1 (loading control) protein levels are shown. Shown are representative results of 2 biological replicates.
(B) Sum1 depletion in the context of ectopic *NDT80* expression in mitosis (refers to Figure 3B, but with all the time points). To express *Ty3* in both meiosis and mitosis, we expressed *NDT80* in sporulating diploid cells (wild type B48, *ty3*Δ B839) and in haploid mitotically dividing cells with and without the Sum1 transcriptional repressor (wild type B477, Sum1-deg B829, and *ty3*Δ B827). Gag3, Sum1 (tagged with 3V5) and Pgk1 (loading control) protein levels are shown. Asterisks show unspecific bands (e.g. band in α-VLP present in *Ty3*Δ). Shown are representative results of ≥ 5 biological replicates.
(C) *Ty3* dimer formation upon Sum1 depletion in the context of ectopic *NDT80* expression in mitosis compared to meiosis (refers to Figure 3B and S3B, but with selection of time points). To express *Ty3* in both meiosis and mitosis, we expressed *NDT80* in sporulating diploid cells (wild type B48, *ty3*Δ B839) and in haploid mitotically dividing cells with and without the Sum1 transcriptional repressor (wild type B477, Sum1-deg B829, and *ty3*Δ B827). In this case, samples were not denatured prior to gel loading (see methods) allow observation of the *Ty3*

RNA dimer formed within the Virus-Like-Particle. *Ty3* dimer (pink arrow), *Ty3* mRNA (black arrow), and *rRNA* (white arrows) are shown. Shown are representative results of 2 biological replicates.

Figure S5: Gag3 protein accumulates in *rim4* truncation mutants and upon Rim4 depletion in meiosis, related to Figure 5

Meiosis was induced in four *NDT80-IN* strains: wild type (B48), Rim4-deg (B1022, Rim4 depletion induced by auxin addition to 1 mM at t = 5.5 h), *rim4Δ138C* (A33845), and *rim4Δ271C* (A33848). Meiotic cells were released from the G2 block by addition of 1 µM β-estradiol at 6 h. Mitotic induction of *NDT80* with Sum1-deg was conducted as in Figure 3B. Gag3, Rim4 (wild type and truncations mutants are tagged with 3V5, Rim4-deg is tagged with FLAG), and Pgk1 (loading control) protein levels are shown. Asterisks show unspecific bands (e.g. band in α-FLAG present in no-tag samples). Shown are representative results of 2 biological replicates.

Figure S6: Mammalian *Gypsy*-derived genes are activated by meiotic transcription factors and regulated by meiotic RNA-binding proteins, related to Figure 6

(A) RNAseq from indicated cell types from adult mouse testes was mapped to the mouse genome, and *Gypsy* family derived elements of the same nature were aggregated together (at the level of RepName using Repeatmasker annotations). The FPKM, fragments per kilobase of transcript per million mapped reads for each *Gypsy* family elements are shown. Biological replicates = 3 for each stage.
(B) RNAseq data from indicated tissue (Marin et al., 2017) and cell types (Lesch et al., 2016) from opossum was analyzed. The FPKM, fragments per kilobase of transcript per million mapped reads for the *M-PNMA* gene is shown. Biological replicates = 2 for each stage.
(C, D) Plots show the distance between each individual MamGyp-int elements **(C)**, or the transcriptional start site of a transcript encompassing a given MamGyp-int element **(D)**, and the nearest Stra8 ChIP-seq peak and Mybl1 ChIP-seq peaks. *Moap1* and *Pnma1* MamGyp-int elements are highlighted in blue and orange.
(E - G) Analysis of retrotransposon sequences in anti-DAZL RNA immunoprecipitation (RIP) from human foetal ovaries (biological replicates = 3). **(E)** Reads were aggregated at the level of RepName using Repeatmasker annotations, and assessed for differential abundance in paired anti-DAZL and IgG RIP. Retrotransposons belonging to the *Gypsy* family are plotted. Asterisk

indicates FDR-adjusted p-value < 0.01 determined by Student's t-test. CPM, counts per million mapped reads. **(F)** Five retrotransposons enriched in Human Fetal Ovary α-DAZL RIP, including MamGyp-int group (in orange, see panel G). **(G)** Human Fetal Ovary α-DAZL RIP enrichment levels for retrotransposons shown in F (in orange) for MamGyp-int and other LTR retrotransposons.

TABLE LEGENDS

Table S1: Laboratory *S. cerevisiae* strains used in this study, related to Figures 1-5 and Figures S1-S5

Table S2: Wild *S. cerevisiae* strains used in this study, related to Figure 1

For these strains, the number of *Ty3* insertions in the genome has been estimated by depth of coverage at a single *Ty3* locus compared to the rest of the genome. Sporulation efficiency was determined by number of asci formed 24h and 72h after sporulation induction. Presence of full-length *Ty3* mRNA was detected by Northern blot as in Figure 1. Standardized names and some relevant information from (Peter et al., 2018) were included.

Figure S1

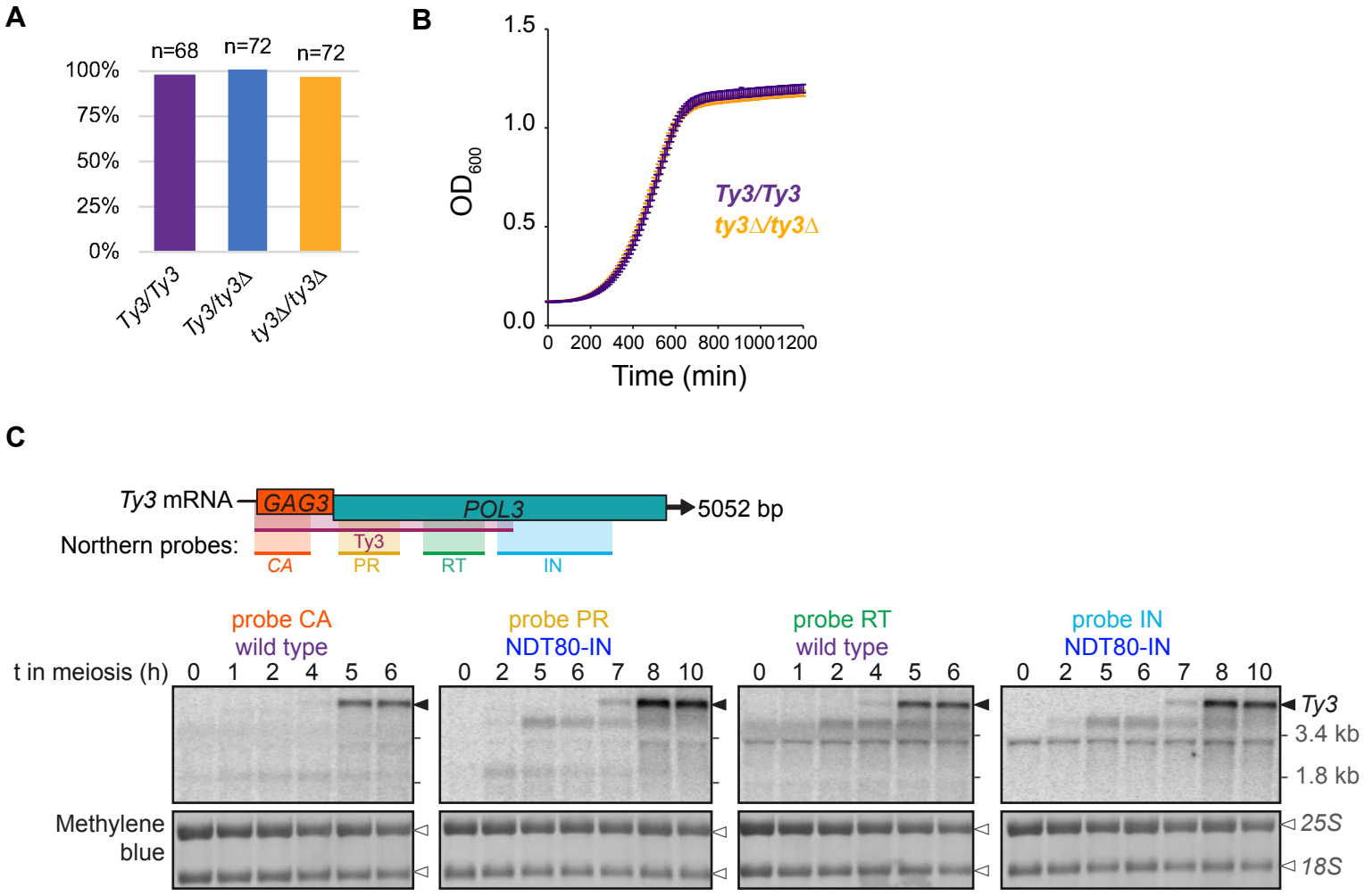
A
n=68
n=72
n=72
100%
75%
50%
25%
0%
Ty3/Ty3
Ty3/ty3Δ
ty3Δ/ty3Δ
B
1.5
1.0
0.5
0.0
OD600
Ty3/Ty3
ty3Δ/ty3Δ
0 200 400 600 800 1000 1200
Time (min)
C
Ty3 mRNA
GAG3
POL3
5052 bp
Northern probes:
Ty3
CA
PR
RT
IN
probe CA
wild type
probe PR
NDT80-IN
probe RT
wild type
probe IN
NDT80-IN
t in meiosis (h)
0 1 2 4 5 6
0 2 5 6 7 8 10
0 1 2 4 5 6
0 2 5 6 7 8 10
Ty3
3.4 kb
1.8 kb
Methylene blue
25S
18S

Figure S2

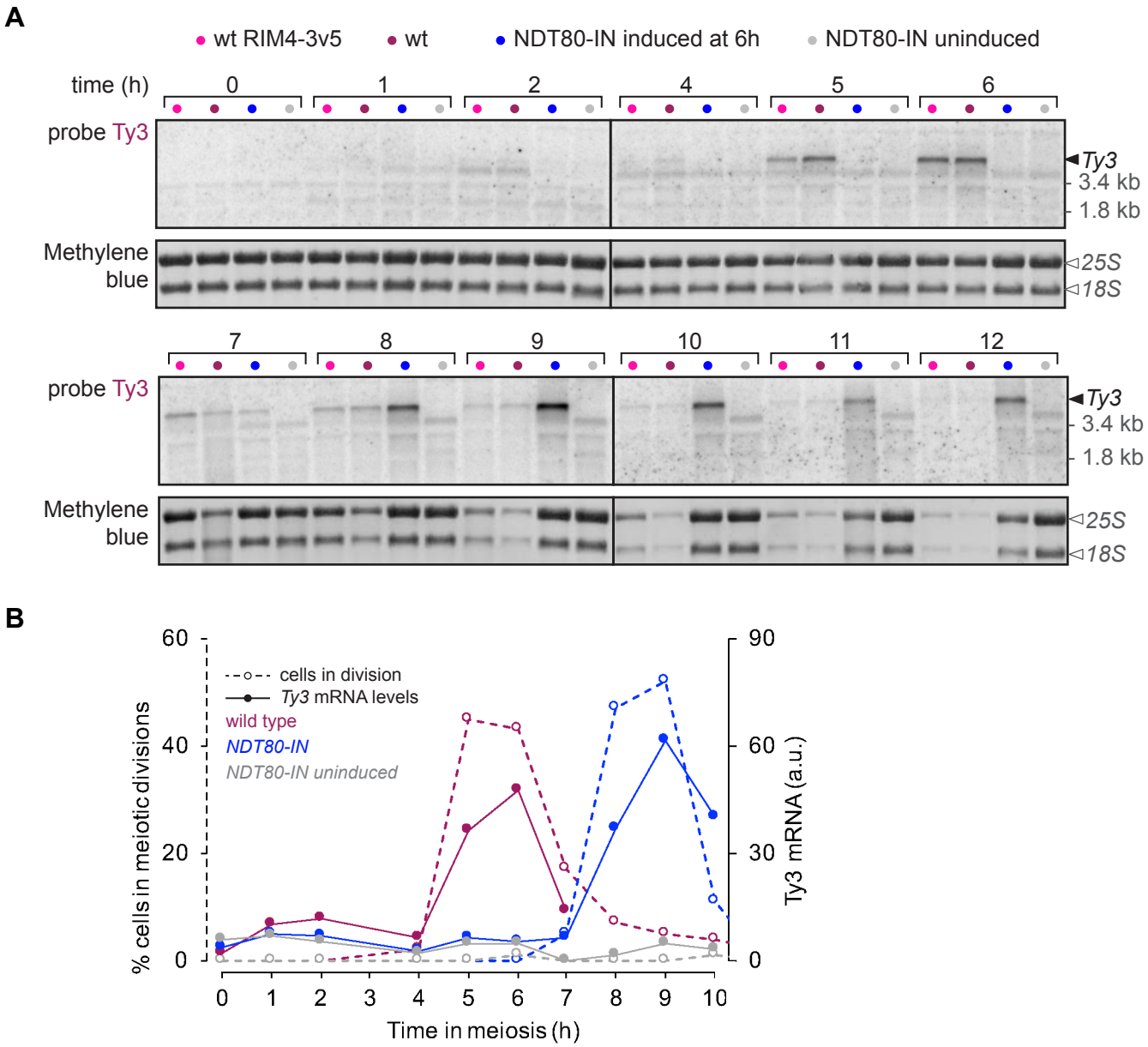
A
wt RIM4-3v5
wt
NDT80-IN induced at 6h
NDT80-IN uninduced
time (h)
0
1
2
4
5
6
probe Ty3
Ty3
3.4 kb
1.8 kb
Methylene blue
25S
18S
7
8
9
10
11
12
probe Ty3
Ty3
3.4 kb
1.8 kb
Methylene blue
25S
18S

B
% cells in meiotic divisions
Ty3 mRNA (a.u.)
cells in division
Ty3 mRNA levels
wild type
NDT80-IN
NDT80-IN uninduced
Time in meiosis (h)

Figure S3

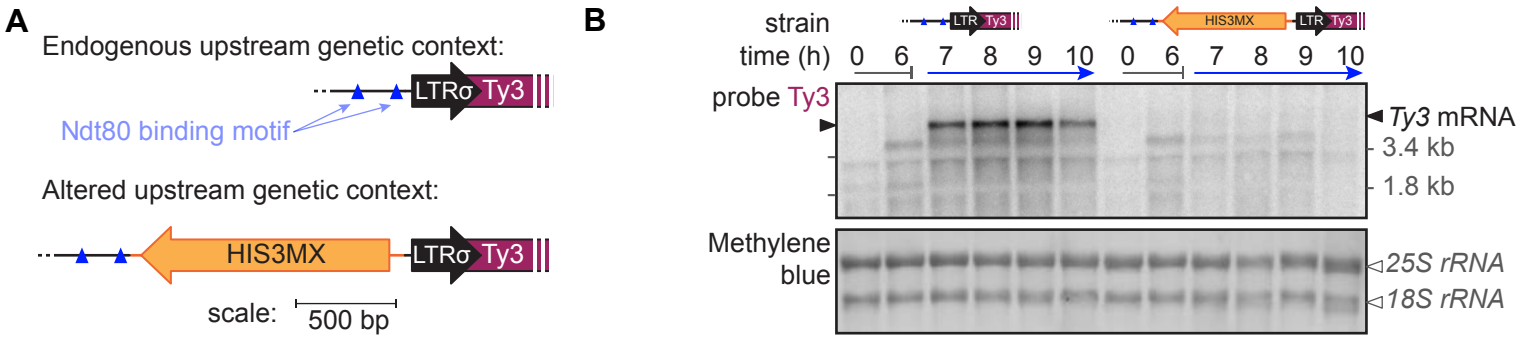
A
Endogenous upstream genetic context:
LTRσ
Ty3
Ndt80 binding motif
Altered upstream genetic context:
HIS3MX
LTRσ
Ty3
scale:
500 bp
B
strain
time (h)
0 6 7 8 9 10 0 6 7 8 9 10
probe Ty3
Ty3 mRNA
3.4 kb
1.8 kb
Methylene blue
25S rRNA
18S rRNA

Figure S4

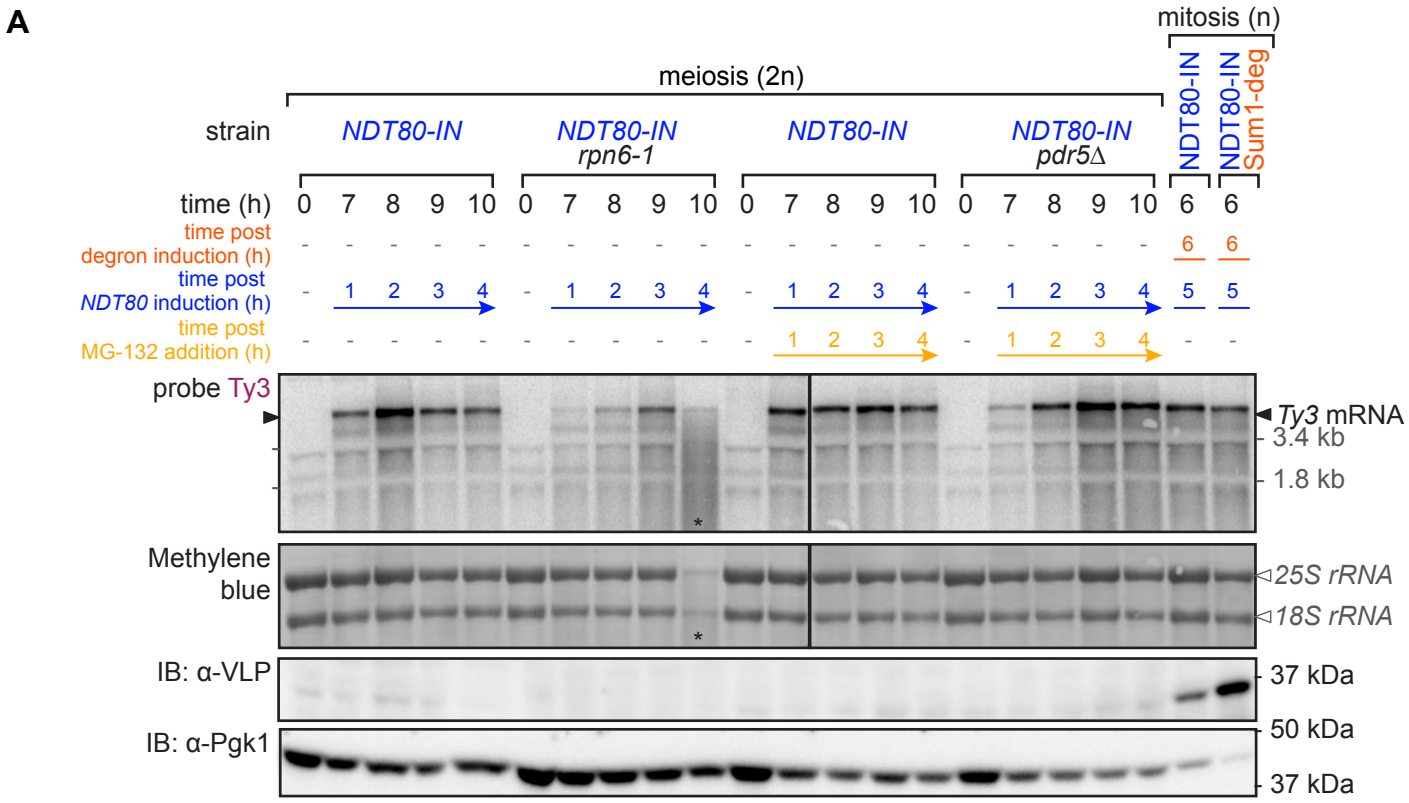
A
mitosis (n)
meiosis (2n)
strain
NDT80-IN
NDT80-IN rpn6-1
NDT80-IN
NDT80-IN pdr5Δ
NDT80-IN
NDT80-IN Sum1-deg
time (h)
time post degron induction (h)
time post NDT80 induction (h)
time post MG-132 addition (h)
probe Ty3
Ty3 mRNA
3.4 kb
1.8 kb
Methylene blue
25S rRNA
18S rRNA
IB: α-VLP
37 kDa
IB: α-Pgk1
50 kDa
37 kDa

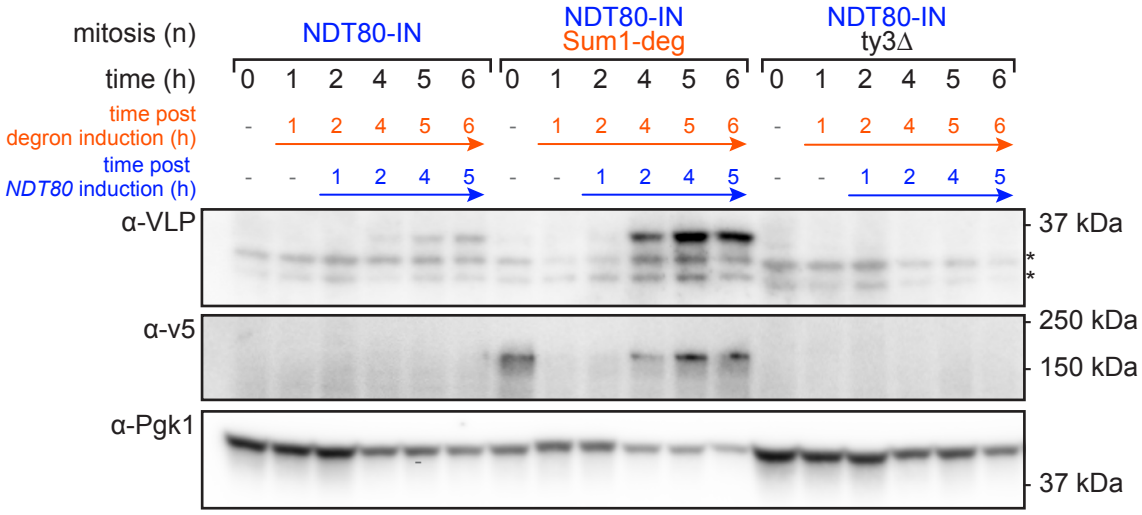
B
mitosis (n)
NDT80-IN
NDT80-IN Sum1-deg
NDT80-IN ty3Δ
time (h)
time post degron induction (h)
time post NDT80 induction (h)
α-VLP
37 kDa
α-v5
250 kDa
150 kDa
α-Pgk1
37 kDa

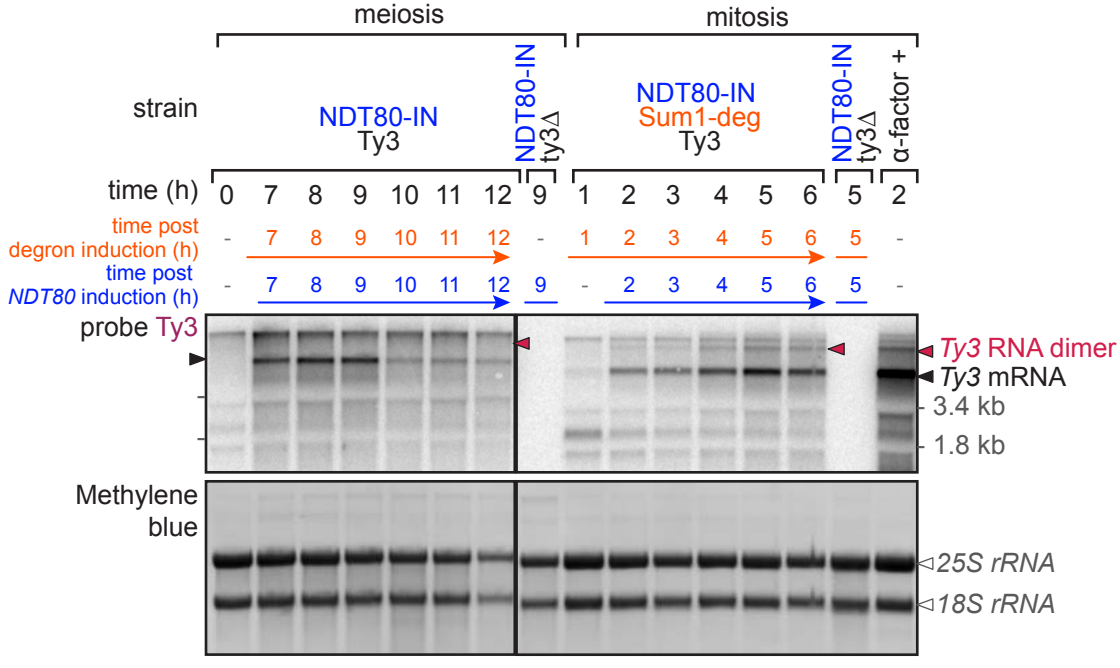
C
meiosis
mitosis
strain
NDT80-IN Ty3
NDT80-IN ty3Δ
NDT80-IN Sum1-deg Ty3
NDT80-IN ty3Δ
α-factor +
time (h)
time post degron induction (h)
time post NDT80 induction (h)
probe Ty3
Ty3 RNA dimer
Ty3 mRNA
3.4 kb
1.8 kb
Methylene blue
25S rRNA
18S rRNA

Figure S5

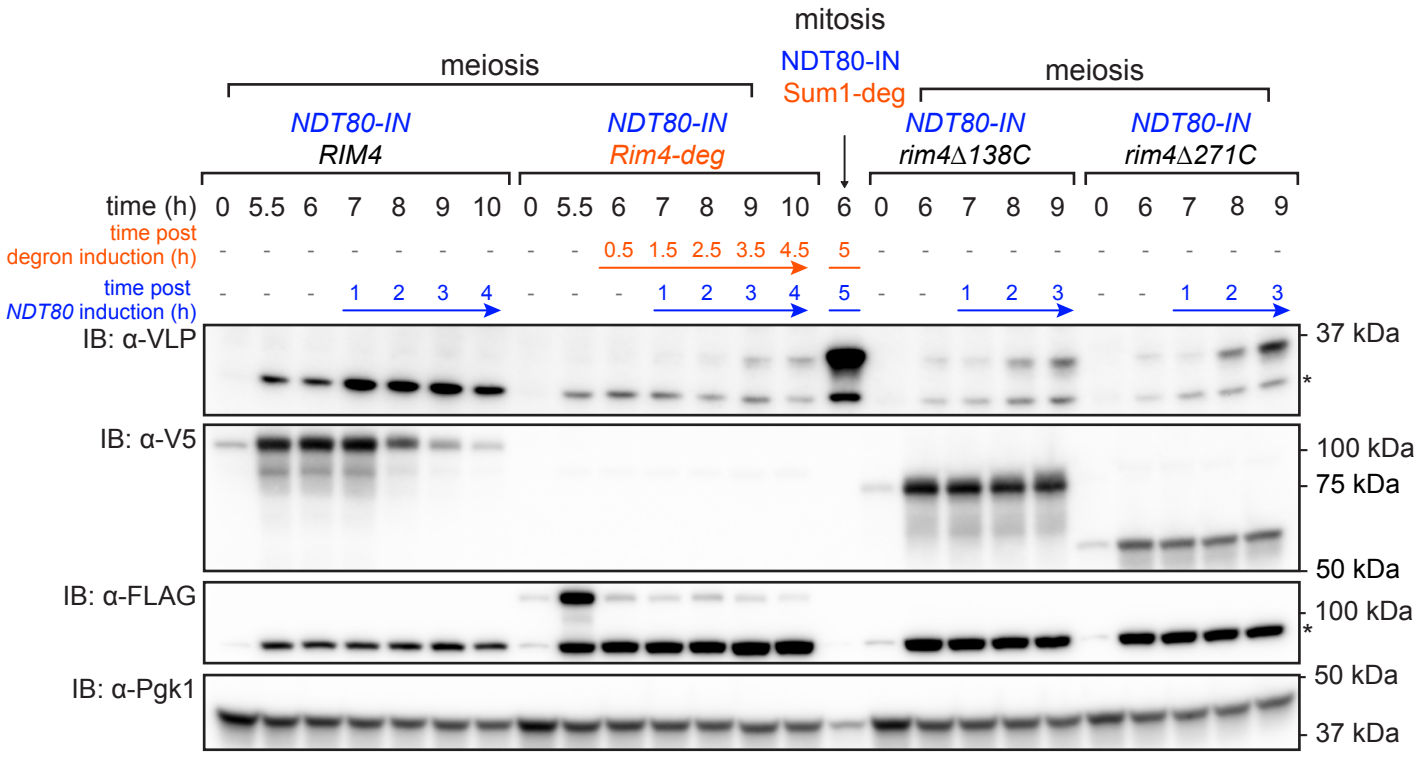
mitosis
meiosis
NDT80-IN
Sum1-deg
meiosis
NDT80-IN
RIM4
NDT80-IN
Rim4-deg
NDT80-IN
rim4Δ138C
NDT80-IN
rim4Δ271C
time (h) 0 5.5 6 7 8 9 10 0 5.5 6 7 8 9 10 6 0 6 7 8 9 0 6 7 8 9
time post degron induction (h) - - - - - - - - - 0.5 1.5 2.5 3.5 4.5 5 - - - - - - - - - -
time post NDT80 induction (h) - - - 1 2 3 4 - - - 1 2 3 4 5 - - 1 2 3 - - 1 2 3
IB: α-VLP
37 kDa
*
IB: α-V5
100 kDa
75 kDa
50 kDa
IB: α-FLAG
100 kDa
*
IB: α-Pgk1
50 kDa
37 kDa

Table S1

Click here to access/download

Supplemental Videos and Spreadsheets

Ty3 table S1.xlsx

Table S2

Click here to access/download

Supplemental Videos and Spreadsheets

Ty3 table S2.xlsx